A PWM CURRENT-FED INVERTER FOR INDUCTION HEATING

ZHIQIN SHU

A PWM CURRENT-FED INVERTER FOR INDUCTION HEATING

by

© Zhiqin Shu, B.Eng.

A thesis submitted to the School
of Graduate Studies in partial fulfillment
of the requirements for the degree of
Master of Engineering

Faculty of Engineering and Applied Science
Memorial University of Newfoundland

October 1992

St. John's Newfoundland Canada

ISBN 0-315-82665-7

Abstract

This thesis presents the description, analysis and implementation of a medium frequency PWM current-fed inverter for induction heating applications. The feasibility of the application of a PWM scheme to the current-fed inverter in this particular field is investigated. The steady-state performance of the system is evaluated by a simulation program which is based on the state-space method of analysis. The analytical results by simulation are verified experimentally on a laboratory set-up of a power level of 100 watts at about 1 kH_z.

The current-fed PWM inverter is designed to achieve the goal of using a simpler control scheme to reduce the power losses and overall maintenance cost. It does not use a stage of controlled rectifier for the output regulation, which has the drawback of injecting large harmonics into the utility system. The overall control strategy is relatively simple, because the control loop does not include the input circuit of the system. The current-fed PWM inverter presented in this thesis shows the possibility of achieving output power regulation by means of both the swept-frequency method and the PWM scheme. A simple IC-based triggering circuit has been developed which can provide the required stable PWM signals in a range wide enough to achieve the goal of control.

Acknowledgements

The author would like to express sincere gratitude to his supervisor, Dr. J.E. Quaicoe for his invaluable guidance, helpful discussions, constant encouragement as well as the financial support throughout the preparation of this thesis.

The author wishes to thank both the Faculty of Engineering and Applied Science and the School of Graduate Studies, Memorial University of Newfoundland, for admitting him into this program and providing adequate financial support as well as all the necessary working facilities. Many thanks are extended to Dr. C.A. Sharpe, Associate Dean of the School of Graduate Studies, for his best understanding and valuable assistance in many ways possible to an international student in the graduate program.

Thanks are also due to the professors, graduate students and other personnel in this university who have provided advice, suggestions and assistance. Dr. G. Sabin is especially appreciated for his valuable discussion and assistance with numerical analysis.

Finally, the author wishes to extend his deep gratitude to his parents, his wife and little daughter in China for their loving encouragement and support as well as their great patience during the whole period of his studies in this university.

Contents

List of Figures

List of Tables

Chapter 1

Introduction

1.1 Power sources for induction heating

Thyristorized inverters are widely used in the induction heating industry. Such furnace power supplies feature high efficiency, high power capability, reasonable power factor into the supply line, and accurate control capability. Because of high power requirements, an important issue with the design of power sources is how to optimize the overall performance of the equipment for a particular task while trying to reduce the unit cost of the equipment at the same time. The latter is meaningful because of the possible massive need of such sources in the industry.

Depending on the characteristics of different materials to be processed and the technology required, the demand for power sources for induction heating/melting applications can be quite distinctive. The working frequency of the systems normally ranges from the supply-line frequencies up to radio frequencies, while the power level could be as low as a few kilowatts, or as high as several megawatts. No single equipment in reality, therefore, could operate over such wide power and frequency ranges, due to the physical limitation.

The power supplies for induction heating fall into four categories, namely the supply-frequency systems, motor-alternator systems, solid-state converter and radio-frequency systems. Their applications are illustrated in Figure 1.1.

These supplies are substantially frequency dependent in terms of power levels. Among them the solid-state inverter systems have virtually replaced the motor-alternators over the past few decades, due to rapid developments in the solid-state devices. The inverter systems comprising SCRs are mainly designed for " medium " frequency applications at high power levels. The term " medium " used in this field is not so clearly defined in the literature [1, 2, 3]. Actually, the frequency of the lower bound of the systems could be close to the supply-line frequency, while the restriction of the frequency on the upper bound with this type of system is determined by the physical limitation of the turn-off time characteristics of the SCRs. Current technology results in an upper frequency of some tens of kilohertz.

Inverter systems can be subdivided into voltage source type (VSI), also known as " voltage-fed " inverters, and current source type (CSI), or " current-fed " inverters, according to their DC inputs characteristics. In the literature, they are also normally identified by their load connection formats, i.e., series inverters which usually correspond to the voltage-fed type, and the parallel inverters that correspond to the current-fed type. Either type has its own particular merits, depending on the applications.

Figure 1.2 shows two typical configurations for VSI and CSI inverters, respectively. Current-fed inverters are fairly common for induction heating, as in many cases the load consisting of the working coil together with the work-piece is tuned in parallel with a

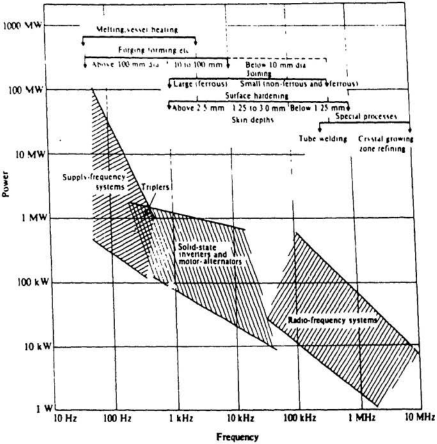

Figure 1.1: Induction heating systems and processes [4].

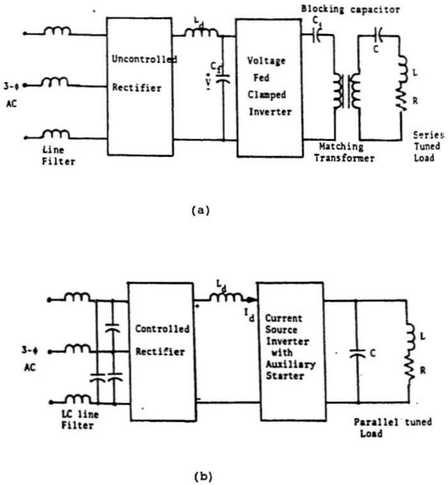

Figure 1.2: Two different inverter configurations [5]: (a) A VSI inverter circuit; (b) A CSI inverter circuit.

compensating capacitor. The purpose of this compensation is to constitute a resonant circuit so as to maximize the power delivery as well as to increase the power factor of the load. More importantly, it can provide the capability of load commutation. In a current source inverter, the actual current source is realized by using a sufficiently large inductor in series with a voltage source to provide a "constant current". This inductor can sometimes provide an instantaneous protection due to a short-circuit on the load. However, this type of inverter usually requires a stage of controlled rectifier for the major regulation of the current fed into the inverter bridge. Six thyristors of large ratings in the case of three-phase supply are required which increases the cost of the whole system. Such a converter may inject large harmonics into the utility system. The power factor could be poor when the load parameters vary during the heating cycle, since phase angle control of the converter is required. Furthermore, two separate triggering circuits to control both the rectifier and the inverter itself are needed. This makes the control tasks unnecessarily complicated. These problem could be solved by regulating the outputs within the inverter rather than using a separate variable DC link. Although many other variations of the inverters have been attempted in recent years, current-fed inverters are still widely used.

The pulse-width-modulation (PWM) technique becomes more and more popular owing to the ever-increasing availability of the microcomputers. It has also been introduced into power converter/inverter systems, mainly for harmonics reduction and output regulation purposes with high efficiency. In the case of induction heating, due to the inherent high power levels and associated high switching losses of the SCRs, the method is not really suitable for the multi-pulse schemes, especially at high frequencies [6]. Another fact is that the effect of the PWM methods may depend on the type of the inverter sources. Normally, fairly sophisticated control efforts are required for realizing the PWM schemes.

1.2 Thesis objectives and outline

A PWM current-fed inverter is proposed. The PWM scheme is to be used to achieve the regulation of the output power of the inverter so as to eliminate the need for using a controlled rectifier for such a purpose. The objectives of the research is to investigate the feasibility of the PWM current-fed inverter for induction heating and to characterize its performance. State-space approach is widely used for both linear and nonlinear system analyses. For inverter systems, it permits a complete design with as many variables and parameters as possible with the help of digital computers. In this thesis, it is proposed to develop a PWM current-fed inverter, adopting the state-space approach to describe the performance of the inverter.

Chapter 2 gives a review of past research on inverters for induction heating. Different schemes including some recent applications in this area are introduced and compared with one another. The PWM technique and numerical means commonly used for the analysis of inverters are also discussed briefly.

In Chapter 3, the description and analysis of the proposed inverter are provided. State-space equations are formulated and solved to obtain the performance of the inverter for steady-state response under varying load parameters. Numerical analysis tools, such as *Runge-Kutta* algorithm and *characteristic roots* method, and subroutines of commercial packages (such as MATLAB, MAPLE and NAG FORTRAN) are used to develop the efficient simulation programs for the solutions to the state-space equations. Performance curves are provided and discussed based on the simulation results.

The implementation of the PWM based triggering circuit for the inverter and experimental verification of the PWM current source inverter are presented in Chapter 4. A design example is given at the end of the chapter.

Finally, Chapter 5 concludes the thesis by pointing out the merits of the proposed inverter and discussing the aspects of a closed-loop control system for this inverter. Future areas of investigation to enhance the system performance are discussed.

Chapter 2

Review of Previous Work

Significant improvements in the power supplies for induction heating facilities have been achieved over the past several decades [4, 7], due to the developments in semiconductor devices of high power ratings, power inverter configurations and the relevant control schemes. The evolution of power inverters has been in two broad ways: better performance by means of new devices, and designated enhancement by advanced techniques like the PWM. However, so far, the PWM technique has not been well developed for induction heating applications, but for the motor drives [8, 9, 10]. Generally speaking, the problem with the development of high-power inverters is how to achieve a simple-structured main circuit of high efficiency with a less complex electronic control circuitry to perform a complicated task. This chapter gives an overview of the previous work on developments of different inverter schemes for induction heating/melting applications. The requirements of an induction heating power supply, principles of both power inverters and the relevant analytical means to determine the performance of induction heating power supplies are discussed. Finally, the concept of the PWM technique proposed in the thesis for the current source inverter is introduced.

2.1 Requirements and modelling of a power inverter for induction heating

In this section an induction heating load is described and modelled mathematically. Major requirements of an induction heating power supply are discussed in terms of its applications.

2.1.1 Electrical characteristics and mathematical modelling of an induction heating load

Induction heating is based on three principles: electromagnetic induction, " skin effect ", and heat transfer. Figure 2.1 (a) shows an actual induction heating furnace which consists of a heating coil and work-piece (billet). The concept of induction heating can be explained with the help of the transformer theory as shown in Figure 2.1 (b) and (c). For an induction heating furnace, a transformer with a single turn and short-circuited secondary winding is used to describe the actual induction heating coil with the load, where the primary winding represents the coil, while the work-piece actually constitutes the single-turn secondary winding [4]. The ratio of the transformer turns is determined according to different applications, such as heating, melting and hardening, and the relevant technology. The load composed of the coil and the work can be modelled equivalently as a combination of an inductance and a resistance in series. It is shown in Figure 2.1 (d), where $L_{eq}(\omega)$ and $R_{eq}(\omega)$ represent the inductance and resistance, respectively, which are functions of frequency. In most analysis it is convenient to define a dimensionless parameter called " quality factor Q " of the load. Referring to Figure 2.1 (d), the Q value

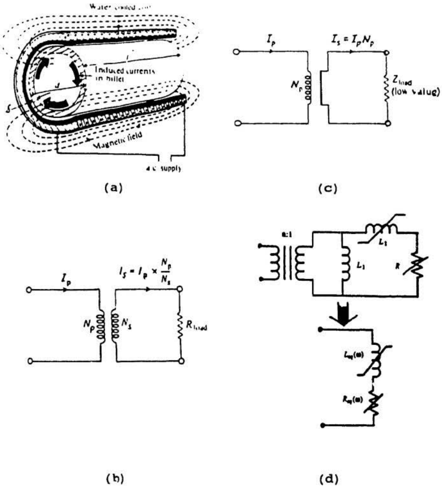

Figure 2.1: Basic concepts of induction heating coil and load [4]. (a) Coil and load. (b) Transformer. (c) Shorted secondary effect. (d) Equivalent electric circuit model of an induction heating coil [5].

of this load can be defined as follows:

$$Q = \frac{\omega L_{eq}(\omega)}{R_{eq}(\omega)}, \tag{2.1}$$

where ω is the frequency of the alternating current flowing through the coil.

The term Q is also used for a resonant circuit. In this case, if a capacitor C is connected in parallel with the coil, a resonant frequency ω_o can be found and the Q is normally defined as:

$$Q_o = \frac{\omega_o L_{eq}(\omega_o)}{R_{eq}(\omega_o)}, \tag{2.2}$$

$$\omega_o \doteq \frac{1}{\sqrt{L_{eq}(\omega_o)C}} \qquad (rad./sec.). \tag{2.3}$$

For different applications, the range of Q values can be from as low as 2, to as high as 20; even for a particular coil with load, the effective Q could vary over a wide range during the heating process [1, 2, 4]. The change in load can also be regarded as impedance and angle changes due to the variation of resonant frequency of the tank when heated [11]. This method is actually compatible with the assumption that Q changes.

The fundamentals and details of the coil design for various applications are available in the literature [2, 4]. It should be pointed out, however, that the effective parameters of the coils in terms of $L_{eq}(\omega)$ and $R_{eq}(\omega)$ can be subject to other factors such as temperature, size and type of the work-pieces. That is why both parameters are modelled as nonlinear impedances, as shown in Figure 2.1 (d). A *matching transformer* would be needed when a power source, if maximum power delivery is desired or some consideration of power ratings of the coils is required . It is common practice in the analysis of inverter circuits to model the whole load using only an $R - L$ circuit. The variation in coil parameters is reflected by the Q values of the coil [1]. The design of the proposed inverter system conducted in this research follows such an assumption, as a complete design of coils with particular load parameters is beyond the scope of this thesis.

2.1.2 Requirements of a power inverter for induction heating

From the literature [1, 4], the main requirements of an induction heating apparatus can be summarized below:

Self-starting capability The processing should be started easily by firing the SCRs without the help of any other auxiliary apparatus. Under some conditions, when Q values of the load of a voltage source inverter are either too high or too low, this kind of inverter has a starting problem. Or for a current source inverter, it cannot be started from " cold ", since at the beginning of the process, there is insufficient voltage across the parallel compensated capacitor. Many methods have been developed and used to help start such an inverter [1, 3].

Substantial load change capability In the heating process, the parameters of the load tend to vary considerably, especially in the case of steel heated through Curie temperatures. A small change in the load parameter is reflected in the whole coil and tank impedance. Besides, abrupt changes in load parameters due to the change of load shape and size, or, in the abnormal condition when a short circuit occurs, should not affect the operation of the inverter system. This is ensured by the control/protection circuitry of the system.

Constant power output To both maintain a rated output power and keep the power supplied to the load to safe operating conditions, effective means for regulation of the output power under wide load variations should be provided. The change during the heating process can normally be expressed as a variation in the Q of the load. Therefore in most cases the design of the power supply is based on the determination of the maximum range over which the Q of the coil will vary.

Generally speaking, regulation of the output power is one of the main objectives of the power supply designers. In fact, the variation of the resonant frequency of the load circuit can also affect the load impedance, and therefore the output power. In this thesis, the analysis is based on the assumption that only Q varies, since this reflects many actual situations.

2.2 Classifications and functions of power inverters

Solid-state static inverters are extensively used today in induction heating applications. The typical environment for the heating process is such that a three-phase supply provides power to the inverter through a DC link. Inverters using SCRs are mainly for medium-frequency applications, while for very high frequency cases SCRs must be replaced by some high-speed power transistors like MOSFETs. There are several types of inverter schemes available. Typically they fall into the following classifications: voltage or current inverters, series/parallel inverters and load-resonant inverters, which are defined differently. The inverter discussed in the thesis corresponds to the type of current source inverter.

2.2.1 Comparison of voltage source (VSI) and current source (CSI) inverters

As the name indicates, a voltage source inverter uses a voltage source as its DC link, while the current source inverter uses such a source together with a large inductor to provide an equivalent " current source ". An example is shown in Figure 1.2 (b). One of the major differences between the two is that the VSI inverter has a stiff DC voltage source. Since this voltage is directly applied to the load, large variation is not desirable. Therefore the regulation of the output power is normally achieved by varying the operating frequency of the inverter. In the CSI inverter, however, the constant current source is obtained by means of a closed-loop current control in the DC link. This control also provides the function of output power regulation in a conventional CSI inverter. Dawson and Jain [2] have conducted a comparison of the two inverters with a conclusion that VSI inverters are better in converter utilization at higher frequencies. The CSI inverters are more rugged and reliable; a momentary short circuit in load does not affect the operation very much. Normally, a closed-loop control system is required to further protect the CSI inverter.

2.2.2 Swept-frequency systems and load-resonant inverters

Davies and Simpson [4] have given a good background knowledge of the solid-state static inverters for induction heating. Two basic inverter systems, namely the *swept-frequency generator* and *load-resonant generator*, have been introduced and discussed, which are shown in Figure 2.2. The two schemes reflect the principles of the power control of the systems: by frequency variation or by variable DC supply at fixed frequency. It should be noted that the actual applications are sometimes the combination of both.

Swept-frequency systems have the following characteristics [4].

- They are used for melting applications at relatively low power levels, and are suitable for high-Q loads;
- due to a large series reactor isolating the loads from the source, they enable a wide range of load impedances to be matched;
- open/short-circuit situations in the load are tolerable;
- a series commutating circuit is used, which causes a constant loss so that the efficiency at reduced power level is low;
- the range of power control is limited by the Q value of the load circuit.

Therefore this type of inverter is quite limited in use with a load of wide Q variation, in terms of the output power regulation. Besides, the power factor of the system could be poor when the load is badly tuned.

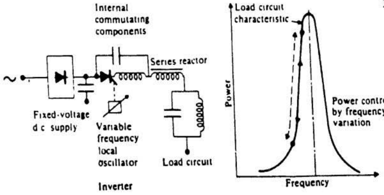

(a)

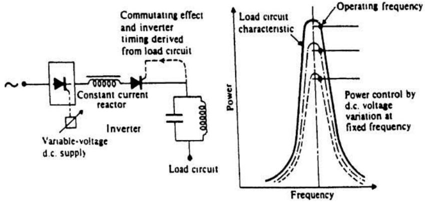

(b)

Figure 2.2: Basic inverter circuits [4]. (a) Swept-frequency generator. (b) Load-resonant generator.

Overcoming the drawbacks of the swept-frequency system, the load-resonant system has the following features.

- It is especially suitable for high power levels, as in through-heating and large melting applications with high efficiency;
- it has less losses particularly under reduced load conditions, and provides large range of power control independent of load Q;
- the output from the load is tapped and fed back as a commutation circuit to turn-off the SCRs.

No auxiliary commutating circuit is needed for load-resonant inverters. A special feature of such circuits is its *extinction time*, as shown in Figure 2.3. This interval t_c begins from the point at which the SCRs (the previously conducting pair) stop conducting, to the point where it is required to block forward voltage, as the thyristors need their *turn-off* time to recover the blocking capability. This is achieved by ensuring that the load phase angle $\phi = \omega_s(t_{overlap}+t_c) \geq \omega_s t_{off}$, $(\omega_s > \omega_o)$, where ω_s and ω_o are the switching frequency and the load resonant frequency, respectively, and t_{off} is referred to as the device turn-off time. Otherwise the inverter will not commutate successfully. It can be seen here that the parameter t_{off} is a decisive factor in limiting the upper operating frequency. Generally speaking, load-resonant systems work more efficiently than the other type, at high power level and operating frequencies, but require more attention to the control strategy.

Since the power control of a load-resonant inverter is realized with a separate DC link, the load could be better tuned whenever the regulation is needed. The power factor of

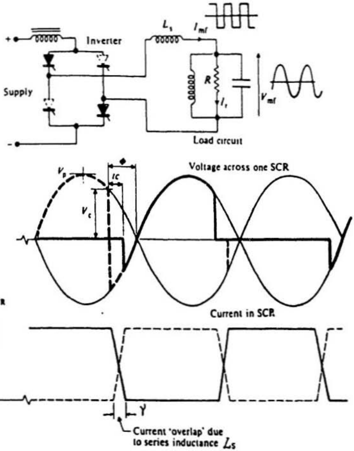

Figure 2.3: Load-resonant commutation [4].

the load circuit is superior to that of the swept-frequency on the average in this regard. From the whole system point of view, it would not be so high as expected. The power factor of the controlled rectifier used in this system is low at reduced DC output level when the conduction angle becomes small. Within a certain limit, load-resonant inverters also possess the capability of regulating the output by frequency variation means.

Both systems described above are of basic types. Load-resonant inverters belong to the current-fed type, or parallel inverters, according to the load configuration. While swept-frequency inverters are considered as a constant-voltage, variable-frequency source in series with an output inductor. In practice, many variations exist that can possibly enhance some of the functions of the basic type.

2.3 Developments of power inverters for induction heating

In 1969, Dewan and Havas [12] published their implementation of a phase and frequency changer with the capacity of 100 kilowatts at around 1 kH_z . This AC-AC converter required three pairs of thyristors, and no DC link is used. Several LC components have been used, apart from the compensating capacitor for the load that are used for commutation purpose. This early attempt of static converter equipment overcame some common difficulties experienced by the motor-generators. Later in 1970 Pelly [1] provided with a detailed practical description of the high frequency power source. He thoroughly discussed the current-fed inverters for induction heating/melting applications. Merits of the parallel, series- parallel and time-sharing schemes were provided. The second type is superior to the first in current dependent commutating capability and easy starting, but causes more stress on the power devices. The time-sharing system was developed to solve the frequency limit problem of current-fed inverters due to the turn-off time restriction of devices, at the cost of more power devices and complexity of the control strategy. The CSI time-sharing inverter also avoided some disadvantages of the voltage-fed type available in the same period of time. Pelly's work related mostly to qualitative descriptions of the working principles of the inverter systems. Few analytical results were provided in the literature to evaluate the performance of the systems.

Revankar and Gadag [13, 14] presented in 1973 and 1974 quantitative analyses of the current-fed parallel and series-parallel inverters using a simplified method. A number of nomograms were made and their use for the choice of circuit components was discussed.

In addition to the wide applications of CSI inverters, efforts have also been made to develop voltage-fed inverters for certain induction heating situation since 1970's. Roda and Revankar [15] investigated a completely different scheme with a voltage source. The emphasis of the analysis was put on the normal working conditions and the available turn-off angle characteristics that were considered to be superior to the CSI type. However, this scheme requires highly accurate closed-loop control in order to achieve the designated performance as well as to avoid its possible abnormal operation.

An important issue with the applications of thyristor inverters for induction heating is how to provide an efficient means of variable DC input so that the outputs of the inverter could be regulated accordingly. In developing an inverter system it would be helpful to find the answers to the following in the first place.

1. During the heating process, to what degree should the load parameters vary, and will any regulation efforts be needed in the inverter stage?

2. What kind of means would be available/adopted for the regulation purpose?

In the literature cited in this section two basic types of regulation methods are adopted in most applications, as described in subsection 2.2.2. However, few performance evaluations of the systems on the power regulation have been provided. Analysis of applications of the PWM technique in CSI power inverters for induction heating are seldom found so far.

2.4 The PWM technique and its potential

The PWM technique is being used extensively in power apparatus applications for better performance, especially in the static converter systems. Voltage-fed PWM inverters are relatively straightforward to build, and current-fed PWM inverters have also been under active investigation [6, 8, 9, 10, 16]. Various PWM schemes are chosen in practice mainly for the following two reasons:

1. providing an efficient means to regulate the inverter outputs, such as the voltage and power;

2. intentionally reducing certain harmonics so as either to make contribution to the specially desired output waveforms, or to decrease the equipment cost by means of easy filtering.

Commonly used PWM strategies include [16]:

- Single-pulse-width modulation (SM)
- Multiple-pulse-width modulation (MPWM)
- Sinusoidal pulse-width modulation (SPWM)
- Modified sinusoidal pulse-width modulation (MSPWM).

Among these, the last three options are in an ascending order to achieve increasing effect of harmonic reduction with the resultant complexity of the same order.

One obvious disadvantage of these schemes, particularly the MPWM and SPWM methods, is that due to the large number of on-off switching of the power thyristors, the switching losses would unavoidably increase. This could be tolerable for motor control applications, where the power level may not be of the most concern and the working frequencies are in most cases fairly low.

The SM method may be chosen for induction heating applications. Due to the normal high-Q nature of the compensated load, the harmonics problem would not be a major concern here. The SM scheme is used for power regulations from power loss considerations. The principal waveforms of the modulation scheme are illustrated in Figure 2.4. By varying δ from 0 to π, the effective output in Figure 2.4 (b), according to Fourier analysis, is given by:

$$v_o(t) = \sum_{n=1,3,5,\ldots}^{\infty} \frac{4V_o}{n\pi} sin\frac{n\delta}{2} sin n\omega t, \tag{2.4}$$

where the item $sin\frac{n\delta}{2}$ controls the output accordingly.

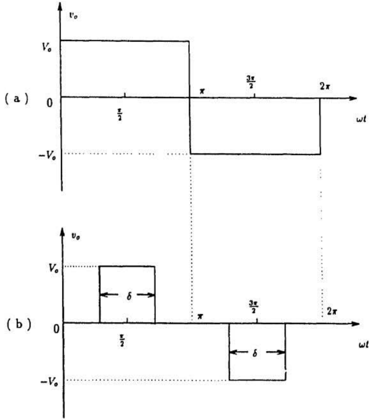

Figure 2.4: Illustration of single pulse-width-modulation [19]. (a) The output waveform without modulation. (b) The modulated output waveform.

To realize the CSI PWM scheme with inverters, some special attention is needed [8, 9, 10]. In almost all the applications that require high power, the actual current source is achieved by using a large inductor in series with a voltage source. Rather than being " constant ", there are variations in the " current source " when the load of the source changes. This fact should be given enough considration.

2.5 Analytical methods and numerical analysis of inverter systems

In the early period of time, basic circuit theory was used to analyze inverter systems. Assumptions and simplifications of circuit equations limited the analysis of performance of the systems. For instance, in Gadag's analysis [13], the working frequency ω_s is selected to be close to the resonant frequency of the load, i.e., the assumption $\omega_s \doteq \omega_o$ should be satisfied. All the results were obtained with the above assumption accordingly. *Fourier series* method was also used for analysis. If the source of the system is not fixed, the analysis will become more difficult. Later Roda and Revankar [15] used state-space method for the circuit analysis, and obtained more accurate results with the resultant simulation programs. They chose the *characteristic roots* method for the computation, rather than the commonly used *Runge-Kutta* algorithm, pointing out that the latter required 2-4 times more CPU time and also had the instability problem. This algorithm, however, results in the equation-oriented programming so that whenever a single parameter is reconsidered, the whole program would need modification. The advantage of this method is its faster speed in terms of CPU time, if partial solutions to the system equations are achieved analytically. The Runge-Kutta algorithm is slow because a large number of iteration is required if a high accuracy is desired. This gets worse especially when either the equations to be solved are of high order or more parameters are under consideration that requires more iterations. So new approaches should be discovered to pave the road to a more efficient computation-based design. Generally speaking, with properly developed programs, both methods mentioned above may result in quite satisfactory outputs.

Chapter 3

Analysis and Simulation of the PWM Current-fed Inverter

This chapter is mainly devoted to the analysis and computer simulation of the proposed medium-frequency PWM current-fed inverter for induction heating applications. The PWM method is supposed to substitute for the function of the conventional controlled rectifier used in a CSI as the variable DC link. The output of the inverter, subject to the wide Q variation of the load, is to be controlled now by two parameters, namely the operating frequency ω_s, and the PWM control angle δ. To stress the effect of the PWM scheme, only a parallel tuned load is considered in the analysis. State-space approach is employed in the formulation of equations for the analysis of the PWM scheme. The simplified analytical method and Fourier series approach mentioned in Chapter 2 are not suitable here for the proposed inverter, because the inverter does not work all the time at the frequency $\omega_s \doteq \omega_o$. For the latter method, since the equivalent current source will not be a real " constant " source, greater error would therefore result. Two simulation methods are employed to obtain the solutions of the state-space equations. The first is based on the most frequently used *Runge-Kutta* algorithm programmed with the help of the commercial package MATLAB. The other uses the *charactrristic roots* method supported by the newly developed MAPLE software and the FORTRAN subroutines in NAG package. The latter is mainly developed for a comparison of the execution speeds by the two methods.

Following the description of the inverter system in Section 3.1 the working principles of the parallel inverter, both with and without the PWM modulation, are explained in Section 3.2; the turn-off time for the successful commutation in both cases is analyzed in detail. Section 3.3 is concerned with the steady-state analysis with which the performance of the inverter is evaluated later. Finally, a brief introduction to the computer simulation (more details are found in Appendix A) and the resultant performance curves are given in Section 3.4. The experimental verification is provided later in Chapter 4.

3.1 Description of the inverter system

Figure 3.1 shows the circuit diagram of the PWM current-fed inverter. Different system functions are described below.

Diode Rectifier This is a $3-\phi$ bridge rectifier comprising six power diodes of large ratings. It converts the AC power from the supply line into a fixed voltage source for the inverter stage. No control circuitry is required for this stage so the implementation is simple. Additional advantages include uniform power factor, and minimum harmonics injected into the utility.

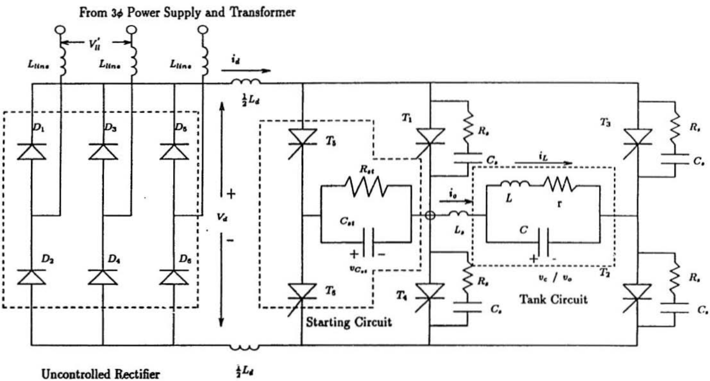

Figure 3.1: Main circuit of a medium-frequency PWM current-fed inverter system

Line Inductor L_{line} This inductor is introduced in each phase of the power supply to limit the maximum amount of the rectifier device current. It also functions as a filter to minimize the harmonics injected into the utility.

Choke L_d It is a type of reactor of large inductance, or choke, which allows DC current component to pass freely. The choke together with the diode rectifier functions as a " current source " which supplies the inverter stage. The inductance of this choke must be sufficiently large so that a relatively smooth current can be maintained. It is dependent on factors such as the tank inductance and the range of Q values of the coil. In order to maintain a relatively smooth current for a wide range of Q values of the coil, the ratio of the reactor inductance to the coil inductance should be at least seventy.

Switches T_1 to T_4 These switches are SCRs that operate at medium frequency and carry substantially high amount of power. The current from the DC link is fed into the bridge inverter composed of these switches and a symmetrical square wave of high frequency current is then pumped into the tank circuit. Snubber circuits with the components R_s and C_s are needed with these devices for protection from excess dv/dt stress.

***di/dt* Inductor L_s** This inductor, including the small inherent wire inductance, limits the di/dt stress of the SCRs. As a result, the current waveforms are not of ideal rectangular wave-shape.

Coil model L and r These two parameters represent the actual coil circuit, which models the furnace, the work-piece and the matching transformer, if used.

Compensating Capacitor C This capacitor is connected in parallel with the coil circuit. It is used to compensate for the inductive effect of the load coil and to improve the overall power factor. Load commutation is also achieved due to a little over compensation to make the whole load circuit capacitive, or to have a leading power factor.

Induction heating loads are of the single phase type. In most applications, 3-ϕ supplies are used to provide higher power and reduce the ripple components in the DC link. The rectifier used in this inverter system is uncontrolled, unlike that of a conventional CSI system, where a closed-loop control is employed to control the DC link current and consequently the output power, inevitably leading to a slow dynamic response. The function of the controlled rectifier in the conventional CSI scheme is now replaced by the PWM scheme which is introduced in the inverter bridge to control the output power. The starting circuit, in a form appropriate for the parallel load[1], operates for only a few cycles until the steady-state operation can be established. Generally speaking, the configuration of this system is the same as that of a conventional CSI inverter, although the two systems do not work in the same pattern.

3.2 Working principles of the inverter circuit

In this section the principle of a CSI circuit with a parallel compensated load is analyzed. Special attention is paid to the commutation process of the PWM scheme.

3.2.1 Turn-off time requirement of a load-resonant CSI without PWM

Some simplification would be necessary to better understand the basic working principle of the load-resonant CSI inverter. A simplified circuit diagram of the inverter is shown in Figure 3.2. The DC source of this inverter is assumed equivalent to a combination of an ideal voltage source of magnitude of E Volts and zero internal impedance. Besides, the snubber components R_s and C_s are neglected in the analysis, since they do not affect the steady-state operation of the circuit.

A complete description of the operation principle of the configuration for induction heating without PWM modulation is available in the literature [1, 3]. Some important points to be ensured for successful operation of the inverter are summarized as follows.

- The constant current i_d provided by the voltage source together with the substantially large smoothing inductor, L_d, is switched in opposite directions through the load circuit by alternatively triggering thyristor pairs T_1, T_2 and T_3, T_4, so that the load current i_o is forced to be of rectangular form. The magnitude of i_d, however, may vary substantially due to the variation of circuit parameters, so it is only *constant* from the transient point of view.

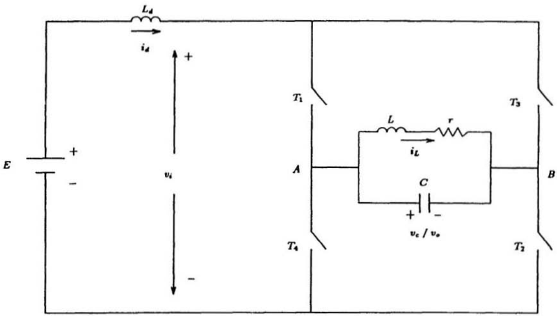

Figure 3.2: Simplified inverter circuit with parallel tuned load.

- The phase angle of the load must appear leading, at the fundamental output frequency. This is ensured by a little overcompensation of the coil by an amount sufficient for the thyristors to commutate. In most cases, this is achieved in practice by operating the inverter at a frequency higher than the resonant frequency of the tank circuit.

As the name indicates, the *starting circuit* is used to build up the required electrical quantities in both the smoothing inductor L_d and the commutation capacitor C, so that the main bridge circuit could be triggered promptly. The principle of operation is discussed in detail in [1]. The circuit used here is of the standard form, which enables the smooth starting of the CSI circuit operation for different Q values. The requirements of the triggering circuit for the starting process is mentioned later in Chapter 4, together with the design of the PWM triggering circuit.

The load commutation phenomenon is the key part in the operation of the inverter bridge. It can be taken to demonstrate the working principle of steady-state mode of the inverter. A full cycle of operation is described in detail in the following paragraph.

Referring to Figure 3.2, suppose T_3 and T_4 are conducting in the steady-state. With both the output current i_o and voltage v_o being negative. Usually the Q value of the coil is reasonably high that a nearly sinusoidal waveform of v_o is obtained. Just before v_o goes to zero, T_1 and T_2 are triggered. Notice that at the instant of triggering this pair of thyristors is forward biased so the pair begins conducting almost at the same time. This action consequently results in the commutation of the other pair, T_3 and T_4, since there are reverse voltages across them at the instant. This process shows the end of negative half cycle of operation and the commencement of the other. The subsequent half cycle occurs in much the same manner. The complete cycle of operation at steady-state of the parallel inverter is illustrated in Figure 3.3.

In Figure 2.3 of Chapter 2, the effect of L_s is emphasized with the output current I_{SCR} during the working cycle. Because of this inductor, the reversely biased pair of thyristors will not cease conducting immediately and therefore all the SCRs will be on during a small interval γ as indicated in the Figure 2.3, which gives rise to the non-ideal rectangular waveform of i_o [13]. Due to the inherent turn-off time characteristics of thyristors, they must be allowed sufficient period of time, t_q, for reliable commutation before they can assume positive voltage again. Otherwise the thyristors would resume conducting as a result.

There are certain critical issues with the load commutation process and hence the circuit operation to be clarified as follows.

1. The thyristor turn-off time t_{off} is the minimum time period required by the nature of the devices to recover their blocking status from the previous conduction. The time t_q given in Figure 3.3 must be larger than t_{off}. t_q is manipulated by the switching frequency ω_s. In the literature, it is usually called *the available turn-off time* of the inverter circuit, which is an important circuit performance index. Sometimes this interval is expressed by a phase angle, as shown in Figure 3.3.

2. From Figure 3.3 it can be seen that t_q is determined by ϕ, phase angle of the tank circuit. The relationship of t_q, t_{off} and ϕ for successful commutation can be expressed as:

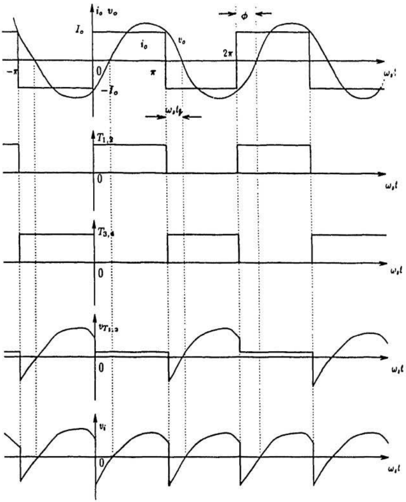

Figure 3.3: Waveforms corresponding to the circuit of Figure 3.2.

$$t_q > t_{off} \tag{3.1}$$

$$\phi = \omega_s t_q \tag{3.2}$$

The maximum working frequency is inversely proportional to the minimum width of the working cycle. It can then be concluded that f_{max} would be mainly limited by the turn-off time t_{off}. This is also because normally t_q only takes a small portion of the period T_s ($T_s = \frac{1}{f_s}$), if too poor a power factor of the load is not expected. For commonly used symmetrical thyristors of large rating, t_{off} is larger than 10 μs.

3. With chosen SCRs in use, a minimum load angle ϕ should always be maintained during the heating process to ensure $t_{q_{min}}$, which is the minimum available turn-off time provided by the system. Basically there are two schemes to realize this [1]. One method is to maintain a fixed phase angle ϕ. In this case, since $\phi = \omega_s t_q$, or equivalently $t_q = \frac{\phi}{w_s}$, demand for changes in w_s means a variation of t_q. To the extreme, $w_{s_{max}}$ will result in $t_{q_{min}}$. Stated another way, a relatively large angle ϕ is required to ensure $t_{q_{min}}$, when ϕ is fixed and the working frequency varies widely during the process. The power factor will therefore be relatively low. The other method maintains a constant turn-off time t_q so that the power factor could be high at low frequencies. This method is commonly used but more efforts in the control strategy is needed than the former [4].

3.2.2 Special commutation process due to the PWM scheme.

As stated earlier, the PWM scheme is proposed to replace the function of controlled rectifier for regulation of the output of the inverter. Specifically, the single pulse-width-modulation (SM) is employed for the inverter. It brings about some special features of the commutation process to be discussed below. Even though there are many discussions about the VSI PWM principles, less attention has been paid to the analysis of the CSI inverter for induction heating. Nor has the side-effect of PWM on the system performance been fully explained.

Figure 3.4 shows the ideal waveforms of the circuit of Figure 3.2 with SM modulation under steady-state operation. To clearly illustrate the PWM mechanism, the effect of L_s is neglected.

The PWM modulation results in two dead zones of the same width in each full cycle of the output current, resulting in the so-called *quasi-square-wave* output waveform. The ratio of the effective part to the full cycle in width of the current can be expressed by the modulation index $p = \frac{\delta}{\pi}$, where δ varies, theoretically, from 0 to π. The amplitude of the output current i_o under different δ could be unequal, but will still be labelled I_o with any particular δ. By the Fourier series theory, the fundamental component of the quasi-square waveform is shown in the figure by the curve of i_{o_1}. The equivalent phase angle of the load now should be the phase difference between i_{o_1} and v_o, if Q is reasonably high.

Suppose at time $\omega_s t = 0$, T_1 and T_2 were conducting until $\omega_s t = \delta$ when T_4 is suddenly triggered to conduct, which is under forward bias. This leads to the commutation of T_2 accordingly. From the waveform of v_{T_1}, it can be seen that T_2 will have sufficient time to

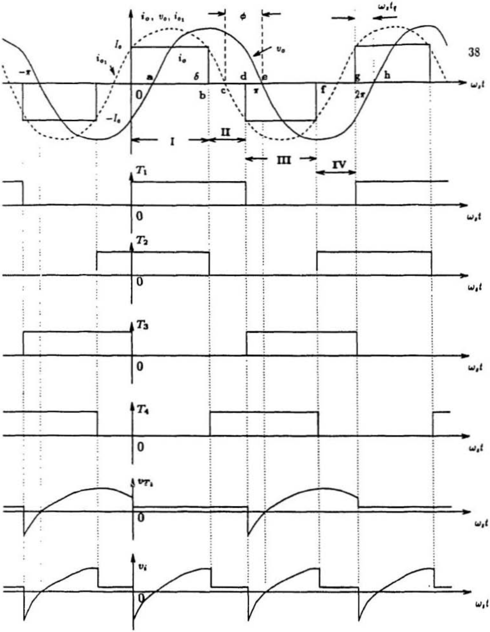

Figure 3.4: Waveforms corresponding to the circuit of Figure 3.2 with the PWM scheme.

turn off, so the short-circuiting of the inverter bridge will not cause a problem with the commutation. At the end of the dead zone, or point d before which both T_1 and T_4 were on, T_3 is fired to start as v_o is still positive. Similarly, T_1 is forced to cease this time. It is fairly evident at point d that v_o cannot be negative, which is the precondition for T_1 to commutate. What is more, this condition should remain until to the point e, to allow for T_1 to successfully turn off. Such a period of time is seen in the figure as that from d to e. The next commutation is supposed to happen to T_4 at f, where another dead zone appears. Turn-off time is not a problem here, either, and at g when T_1 is triggered, T_3 is commutated as a result. So far a complete cycle of operation has been described. Again something important and special with the PWM operation of the CSI circuit of Figure 3.2 should be pointed out below.

1. The basic difference of operations between the PWM scheme and that without PWM is that *each* thyristor is triggered individually, according to certain order, to obtain the quasi-square waveform for output regulation. So four different triggering signals must be provided.

2. The above discussion shows that the load phase angle at the fundamental frequency, ϕ_1, should always be greater than the device turn-off angle. It is clear from Figure 3.4 that the angle should cover from point c to e, not just d to e. This is because there is a dead zone between the turning-off of T_2 and the starting of T_3. If the zero-crossing of v_o is earlier than e, T_1 will resume conduction again, resulting in an abnormal state, even though the total phase angle is already larger than t_{off}. The relationship now could be explained clearly by the following equations:

$$t_q > t_{off} \tag{3.3}$$
$$\phi = w_s t_q + \frac{\pi - \delta}{2} \tag{3.4}$$

3. Equation 3.4 implies that the power factor of the tank could be lower than that without PWM, if the same turn-off time is required, because in the latter case variable DC link is available so ϕ can be smaller. While the overall equivalent power factor could be as satisfactory because of the effect of PWM scheme. This is observed in the simulation results in Section 3.3.5. Equation 3.4 shows that lower power factor is the cost of using PWM. This is an importa . point to be noticed when dealing with such a circuit with PWM.

Unlike voltage-fed inverters, the DC input of which is fixed regardless of the variation of the system parameters, the am. ˈitude of the output current, I_o in the PWM scheme, is a function of certain parameters, such as Q, δ and w_s, and the analysis and control of a CSI PWM inverter have to consider variations in these parameters. The effect is discussed again in the next section.

3.3 State-space analysis of the inverter system

The state-space approach is capable of handling analyses for both linear and nonlinear complex systems with highly accurate results. For the analysis of inverter systems of simple configuration or with relatively straightforward working principles, other methods, such as the *simplified analytical method* and *Fourier series analysis*, can be employed.

However, these methods are not suitable for the inverter system proposed in this thesis. The former method is intended to use certain simplification, such as $\omega_s \doteq \omega_o$, during the derivation of the solutions. Therefore complex calculations can be avoided and a relatively simple set of equations can be obtained for the solutions. For the PWM CSI inverter, this approximation is not valid. The Fourier Series analysis method may be applied to the PWM CSI inverter. However, because the magnitudes of the current source vary with the load parameters, the analysis becomes much more complicated.

The state-space analysis is conducted to obtain various performance curves with which the behaviour of the proposed system is thoroughly evaluated. Necessary equations or relationships are established for the selection of system components. To mainly describe the performance characteristic of the system, the computer simulation is based on a simplified circuit configuration (a third-order system). In addition, normalization (per unit system) is adopted throughout the analysis without the loss of generality.

The detailed discussion of the starting circuit used in the system of Figure 3.1 can be found in the literature [1].

3.3.1 Simplifying assumptions

As a common practice, some basic assumptions are made with the circuit of Figure 3.2 as follows:

1. thyristors and power diodes are ideal and lossless switches, with zero voltage drops in conducting state and zero current in the off state;

2. the AC source is a three-phase voltage source with fixed magnitude and frequency;

3. all the passive components are linear: inductors and capacitors are lossless;

4. the effects of the snubber circuits and starting circuit are neglected;

5. no matching transformer is used in the analysis.

Since the input line inductance L_{line} practically exists, or sometimes it is intended to introduce a relatively large amount of such inductance into the circuit, its influence is considered in the analysis. The three-phase voltage power supply with the secondary line-to-line voltage V'_{ll} and L_{line}, at the line frequency ω_i, is equivalently expressed as a DC voltage source with an equivalent resistance R_i. Referring to Figure 3.1, the magnitude of the source is given by [17]:

$$V_d = E - \frac{3\omega_i L_{line}}{\pi} I_d. \tag{3.5}$$

where $E = 1.35V'_{ll}$ and R_i equals to $\frac{3\omega L_{line}}{\pi}$. Together with the assumption made above, a simplified circuit of the inverter system shown in Figure 3.1 is illustrated in Figure 3.5.

3.3.2 Continuous mode of operation

For a current source inverter, the current fed into the inverter bridge is forced to be constant due to the large inductor, L_d, between the DC power supply and the bridge. Therefore the inverter has only one mode of operation, namely the continuous mode. This mode includes four distinct intervals with the PWM scheme. Respective equivalent circuits and waveforms in a complete cycle are shown in Figures 3.6 and 3.4(e.g. from the origin to the point of g in fig. 3.4).

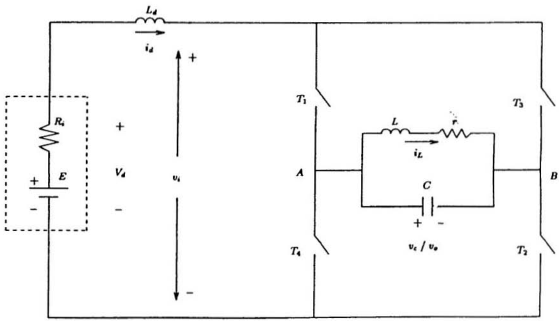

Figure 3.5: Simplified circuit for state-space analysis.

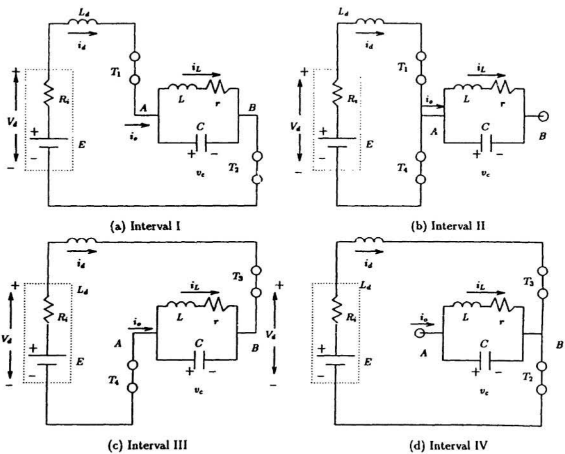

Figure 3.6: Equivalent circuits of the four intervals in the continuous mode of operation.

Interval I During this interval, thyristors T_1 and T_2 are conducting. The output current i_o flowing through the load circuit is positive and remains constant throughout. This induces a nearly sinusoidal waveform of output voltage v_o, or v_c, if the Q value of the tank is not too low To satisfy the commutation condition, v_o must lag i_o by an angle of φ. The width of interval I is controlled by adjusting δ ($0 \le \delta \le \pi$), which affects the output level.

Interval II This is a dead zone of i_o, forming part of the quasi-square-wave. It is achieved at the end of interval I by turning on thyristor T_4 and consequently forcing T_2 to commutate. The tank current is isolated from the DC link during this interval.

Interval III According to the symmetrical operation, T_3 and T_4 are conducting much the same as explained for interval I, except that i_o is negative. v_o at this time transfers from positive to negative, allowing for the same amount of angle from the intersection of interval II and III to give the required turn-off time.

Interval IV Another dead zone appears as thyristor T_2, on the same side of the bridge with T_3, is triggered causing T_4 to cease conducting.

Even though i_o is of a quasi-square-wave pattern, the amplitudes of i_d, and i_o, change substantially, with the variation of circuit parameters such as Q, ω_s or δ.

It is noticed that in the case of $\delta = \pi$, no dead zone is present and the operation of the PWM CSI inverter becomes a non-PWM type. These two systems are analyzed and compared in the thesis, under the assumption that the DC inputs are the same.

3.3.3 Normalization of the system parameters

Per unit system is a useful tool for analyzing power systems. It results in normalized system parameters while providing general results for evaluating a system's performance. In this subsection, all the quantities and parameters used in the analysis are normalized and, whenever necessary, explained.

The resonant frequency of the system, ω_o, and the quality factor of the load circuit of Figure 3.2 at resonance are given by [20]:

$$\omega_o = \sqrt{\frac{1}{LC} - \frac{r^2}{L^2}} \qquad rad/sec., \tag{3.6}$$

and

$$Q_o = \frac{\omega_o L}{r}. \tag{3.7}$$

Since in the actual case, Q is usually high, equation 3.6 can be rewritten as

$$\begin{aligned} \omega_o &= \sqrt{\frac{1}{LC}}\sqrt{1 - \frac{1}{Q_o^2}} \\ &\doteq \sqrt{\frac{1}{LC}} \qquad rad/sec. \end{aligned} \tag{3.8}$$

Then ω_o is chosen as the base frequency

$$\omega_B = \omega_o \qquad rad/sec \qquad (\ 1\ p.u.) \tag{3.9}$$

and the operating frequency is defined as ω_s.

The tank resistance r is used as the base impedance

$$R_B = r \qquad Ohms \qquad (\ 1\ p.u.). \tag{3.10}$$

With reference to Figure 3.5, the amplitude of the equivalent DC source $E = 1.35V_H'$ is taken as the base voltage

$$V_B = E \qquad Volts \qquad (\ 1\ p.u.). \tag{3.11}$$

The other quantities can be derived from the bases above. The base current and power are then given as

$$\begin{aligned} I_B &= \frac{V_B}{R_B} \\ &= \frac{E}{r} \qquad Amps \qquad (\ 1\ p.u.), \end{aligned} \tag{3.12}$$

$$\begin{aligned} P_B &= \frac{V_B^2}{R_B} \\ &= I_B^2 R_B \qquad Watts \qquad (\ 1\ p.u.). \end{aligned} \tag{3.13}$$

It should be noted that these two bases are Q-related because they include the coil resistance r.

Two bases related to angle/time are also selected to evaluate the turn-off time and the power factor characteristics. If θ stands for any phase angle, the base time and base angle are defined by

$$t_H = \frac{\pi}{\omega_o}$$
$$= \frac{1}{2f_o} \qquad (\ 1\ p.u.), \tag{3.14}$$
$$\theta_H = \frac{\theta}{\pi} \qquad (\ 1\ p.u.). \tag{3.15}$$

In the following analysis, all the normalized quantities are designated using over-lined signs as, for instance, $\overline{\omega} = \frac{\omega_s}{\omega_o}$.

3.3.4 Formulation of system equations using state-space approach

In this part of the analysis, the necessary equations required for the computer simulation are derived by employing the state-space method. This approach gives more accurate results than other means commonly used. The effects of many factors changing from time to time, such as those due to PWM modulation, and variations of system parameters ω_s, Q and so on can be easily observed and discussed. Both transient and steady-state responses of the inverter system can be obtained at the same time. Only the steady-state solutions are considered in this section with an aim to produce performance curves for evaluation of the system and selection of the system components.

In Figure 3.5, i_d, i_L and v_c are chosen as state variables. State equations for interval I, with the notation of positive direction of each variables, are found accordingly:

$$v_d = L_d \frac{di_d}{dt} + v_c. \tag{3.16}$$

$$\frac{di_L}{dt} = -\frac{r}{L}i_L + \frac{1}{L}v_c \tag{3.17}$$

and

$$\frac{dv_c}{dt} = \frac{1}{C}i_d - \frac{1}{C}i_L. \tag{3.18}$$

Since i_d is assumed to be constant, so $v_d \doteq V_d$ and $i_d \doteq I_d$. Using equation 3.5, v_d is given by

$$\begin{aligned} v_d &= E - \frac{3\omega_i L_{line}}{\pi} I_d \\ &\doteq E - \frac{3\omega_i L_{line}}{\pi} i_d \end{aligned} \tag{3.19}$$

or

$$\frac{di_d}{dt} = -\frac{3\omega_i L_{line}}{\pi L_d} i_d - \frac{1}{L_d}v_c + \frac{1}{L_d}E \tag{3.20}$$

When interval I is over, the load is isolated from the DC link, as shown in Figure 3.6 (b) for interval II. The corresponding equations during this interval are given by

$$v_d = L_d \frac{di_d}{dt} \tag{3.21}$$

or

$$\frac{di_d}{dt} = -\frac{3\omega_i L_{line}}{\pi L_d} i_d + \frac{1}{L_d}E, \tag{3.22}$$

and

$$\frac{di_L}{dt} = -\frac{r}{L}i_L + \frac{1}{L}v_c, \tag{3.23}$$

$$\frac{dv_c}{dt} = -\frac{1}{C}i_L. \tag{3.24}$$

Interval III is described with a configuration as that in Figure 3.6 (a), except that the load is reversely connected to the DC link. The equation satisfying this period can be obtained easily from equations 3.24 to 3.18 by the positive signs of both i_L and v_c:

$$\frac{di_d}{dt} = -\frac{3\omega_i L_{line}}{\pi L_d} i_d + \frac{1}{L_d} v_c + \frac{1}{L_d} E, \tag{3.25}$$
$$\frac{di_L}{dt} = -\frac{r}{L} i_L + \frac{1}{L} v_c, \tag{3.26}$$
$$\frac{dv_c}{dt} = -\frac{1}{C} i_d - \frac{1}{C} i_L. \tag{3.27}$$

The equations for interval IV are obtained similarly as

$$\frac{di_d}{dt} = -\frac{3\omega_i L_{line}}{\pi L_d} i_d + \frac{1}{L_d} E, \tag{3.28}$$
$$\frac{di_L}{dt} = -\frac{r}{L} i_L + \frac{1}{L} v_c, \tag{3.29}$$
$$\frac{dv_c}{dt} = -\frac{1}{C} i_L. \tag{3.30}$$

All the equations for the four intervals can be rearranged into a set of general expressions given by

$$\frac{di_d}{dt} = -\frac{3\omega_i L_{line}}{\pi L_d} i_d - \frac{m}{L_d} v_c + \frac{1}{L_d} E, \tag{3.31}$$
$$\frac{di_L}{dt} = -\frac{r}{L} i_L + \frac{1}{L} v_c, \tag{3.32}$$
$$\frac{dv_c}{dt} = \frac{m}{C} i_d - \frac{1}{C} i_L, \tag{3.33}$$

where

$$k_1 = \frac{L_d}{L_{line}} \tag{3.34}$$
$$k_2 = \frac{\omega_o}{\omega_i} \tag{3.35}$$

$$k_3 = \frac{L_d}{L} \tag{3.36}$$

$$\overline{\omega} = \frac{\omega_s}{\omega_o} \tag{3.37}$$

and

$$m = \begin{cases} 1, & \text{for interval I} \\ 0, & \text{for intervals II and IV} \\ -1, & \text{for interval III} \end{cases} \tag{3.38}$$

Using the $\omega_s t$ as the time axis, equations 3.31 to 3.33 become

$$\frac{di_d}{d(\omega_s t)} = -\frac{3}{k_1 k_2 \pi \overline{\omega}} i_d - \frac{m}{k_3 \overline{\omega} \omega_o L} v_c + \frac{1}{k_3 \overline{\omega} \omega_o L} E, \tag{3.39}$$

$$\frac{di_L}{d(\omega_s t)} = -\frac{r}{\overline{\omega} \omega_o L} i_L + \frac{1}{\overline{\omega} \omega_o L} v_c, \tag{3.40}$$

$$\frac{dv_c}{d(\omega_s t)} = \frac{m}{\overline{\omega} \omega_o C} i_d - \frac{1}{\overline{\omega} \omega_o C} i_L \tag{3.41}$$

Normalizing equations 3.39 and 3.40 with respect to the base current I_B and equation 3.41 with respect to the base voltage E gives

$$\frac{d\overline{i_d}}{d(\omega_s t)} = -\frac{3}{k_1 k_2 \pi \overline{\omega}} \overline{i_d} - \frac{m}{k_3 \overline{\omega} Q} \overline{v_c} + \frac{1}{k_3 \overline{\omega} Q}, \tag{3.42}$$

$$\frac{d\overline{i_L}}{d(\omega_s t)} = -\frac{1}{\overline{\omega} Q} \overline{i_L} + \frac{1}{\overline{\omega} Q} \overline{v_c}, \tag{3.43}$$

$$\frac{d\overline{v_c}}{d(\omega_s t)} = \frac{m}{\overline{\omega}/Q} \overline{i_d} - \frac{1}{\overline{\omega}/Q} \overline{i_L} \tag{3.44}$$

Equations 3.42 to 3.44 can be written in the matrix form as

$$\frac{d}{d(\omega_s t)} \begin{bmatrix} \overline{i_d} \\ \overline{i_L} \\ \overline{v_c} \end{bmatrix} = \begin{bmatrix} -\frac{3}{k_1 k_2 \pi \overline{\omega}} & 0 & -\frac{m}{k_3 \overline{\omega} Q} \\ 0 & -\frac{1}{\overline{\omega} Q} & \frac{1}{\overline{\omega} Q} \\ \frac{m}{\overline{\omega}/Q} & -\frac{1}{\overline{\omega}/Q} & 0 \end{bmatrix} \times \begin{bmatrix} \overline{i_d} \\ \overline{i_L} \\ \overline{v_c} \end{bmatrix} + \begin{bmatrix} \frac{1}{k_3 \overline{\omega} Q} \\ 0 \\ 0 \end{bmatrix} \tag{3.45}$$

with initial conditions at $\omega_s t = 0$ assumed as

$$\frac{d}{d(\omega_s t)} \begin{bmatrix} \overline{i_d} \\ \overline{i_L} \\ \overline{v_c} \end{bmatrix} = 0 \tag{3.46}$$

Equation 3.45 is the only equation necessary to perform both the transient and steady-state simulation. Once k_1 , k_2 and k_3 are decided, the system outputs can be fully evaluated in terms of parameters of Q , ω_s and δ.

3.3.5 Numerical solutions of the system equations

The solutions to the state variables $\overline{i_d}$, $\overline{i_L}$ and $\overline{v_c}$, are normally solved numerically by computer simulation involving the solution of equation 3.45 . These variables can sufficiently describe the dynamic behaviour of the system. Based on the steady- state part of the solutions of the variables, the output behaviour of the system in the steady-state can be obtained. It is evaluated based on the discrete data of the simulation results over a complete cycle of operation. This is achieved with the *integration of functions* method introduced in [18]. Numerical integration, or *quadrature*, in this particular application is based on adding up the value of the integrand at a sequence of abscissas within the range of integration.

An *alternative extended Simpson's rule* [18] is used for integration of the discrete data. The formula is expressed as

$$\begin{aligned} \int_{x_1}^{x_N} f(x)dx &= h[\frac{17}{48}f_1 + \frac{59}{48}f_2 + \frac{43}{48}f_3 + \frac{49}{48}f_4 + f_5 + f_6 + ... \\ &+ f_{N-4} + \frac{49}{48}f_{N-3} + \frac{43}{48}f_{N-2} + \frac{59}{48}f_{N-1} + \frac{17}{48}f_N], \end{aligned} \tag{3.47}$$

where a sequence of abscissas, denoted $x_0, x_1, \dots, x_N$, is spaced apart by a constant step h,

$$x_i = x_0 + ih \qquad i = 0, 1, \dots, N \tag{3.48}$$

and

$$f(x_i) \equiv f_i \tag{3.49}$$

is exactly known at the x_i's. It should be noted that the selection of h can be based on the choice of step size used in the simulation where the discrete data come from.

Steady-state output and performance index

Applying the Simpson's rule to the data of the results of variables $\overline{i_d}$, $\overline{i_L}$ and $\overline{v_c}$ in a period, $k_1, k_2, \dots, k_N$ or $0 \leq \omega_s t \leq 2\pi$, all the output quantities and some performance indices are obtained as follows:

<u>Mean DC link current</u> i_d is almost constant and can be found as

$$\overline{I}_{d_{ave}} = \frac{1}{N}\sum_{k=1}^{N}\overline{i_d}(k) \qquad (\ p.u.). \tag{3.50}$$

<u>RMS coil current</u> The RMS value of $\overline{I_L}$ is defined as

$$\overline{I}_{L_{rms}} = \sqrt{\frac{1}{2\pi}\int_0^{2\pi}\overline{i_L}^2 d(\omega_s t)} \qquad (\ p.u.). \tag{3.51}$$

Using equation 3.47 gives

$$\overline{I}^2_{L_{rms}} = \frac{h}{2\pi \times 48}[17\overline{i_L}^2(k_1) + 59\overline{i_L}^2(k_2)$$

$$
\begin{aligned}
&+ \quad 43\overline{i_L}^2(k_3) + 49\overline{i_L}^2(k_4) + \overline{i_L}^2(k_5) \\
&+ \quad \overline{i_L}^2(k_6) + \ldots + \overline{i_L}^2(k_{N-4}) + 49\overline{i_L}^2(k_{N-3}) \\
&+ \quad 43\overline{i_L}^2(k_{N-2}) + 59\overline{i_L}^2(k_{N-1}) + \overline{i_L}(k_N)] \quad (\ p.u.)
\end{aligned} \tag{3.52}
$$

and additionally

$$\overline{I}_{L_{max}} = | \ \overline{i_L} \ | \qquad (\ p.u.). \tag{3.53}$$

Inverter output power Only the resistance r in the coil consumes real power. Since r is selected as the base resistance,

$$\overline{P_o} = \overline{I}^2_{L_{rms}} \qquad (\ p.u.). \tag{3.54}$$

RMS voltage of Capacitor C Similar to equation 3.52, this voltage is expressed as

$$
\begin{aligned}
\overline{V}^2_{c_{rms}} \quad &= \quad \frac{h}{2\pi \times 48}[17\overline{v_c}^2(k_1) + 59\overline{v_c}^2(k_2) \\
&+ \quad 43\overline{v_c}^2(k_3) + 49\overline{v_c}^2(k_4) + \overline{v_c}^2(k_5) \\
&+ \quad \overline{v_c}^2(k_6) + \ldots + \overline{v_c}^2(k_{N-4}) + 49\overline{v_c}^2(k_{N-3}) \\
&+ \quad 43\overline{v_c}^2(k_{N-2}) + 59\overline{v_c}^2(k_{N-1}) + \overline{v_c}(k_N)] \quad (\ p.u.)
\end{aligned} \tag{3.55}
$$

and also the maximum voltage is given by

$$\overline{V}_{c_{max}} = | \ \overline{v_c} \ | \qquad (\ p.u.). \tag{3.56}$$

Output current of the load The output current of the load circuit $\overline{i_o}$ determines the current rating of thyristors in the inverter bridge and is found as follows:

$$\overline{i_o} = \overline{i_L} + \overline{i_c} \qquad (\ p.u.) \tag{3.57}$$

and

$$\overline{I}_{o_{rms}} = \sqrt{\frac{1}{2\pi}\int_{k_1}^{k_N} \overline{i_o}^2(k)dk} \qquad (\ p.u.). \tag{3.58}$$

Referring to equation 3.44, $\overline{i_c}$ can be found as

$$\overline{i_c} = \frac{\overline{\omega}}{Q}\frac{d\overline{v_c}}{d(\omega_s t)} \qquad (\ p.u.) \tag{3.59}$$

and therefore,

$$\overline{i_o} = \overline{i_L} + \frac{\overline{\omega}}{Q}\frac{d\overline{v_c}}{d(\omega_s t)} \qquad (\ p.u.), \tag{3.60}$$

$$\begin{aligned} \overline{I}^2_{o_{rms}} &= \frac{h}{2\pi \times 48}[17\overline{i_o}^2(k_1) + 59\overline{i_o}^2(k_2) \\ &+ 43\overline{i_o}^2(k_3) + 49\overline{i_o}^2(k_4) + \overline{i_o}^2(k_5) \\ &+ \overline{i_o}^2(k_6) + ... + \overline{i_o}^2(k_{N-4}) + 49\overline{i_o}^2(k_{N-3}) \\ &+ 43\overline{i_o}^2(k_{N-2}) + 59\overline{i_o}^2(k_{N-1}) + \overline{i_o}(k_N)] \ \ (\ p.u.). \end{aligned} \tag{3.61}$$

Power factor of the load The power factor of the tank circuit can be obtained with the available output quantities as [17]:

$$\begin{aligned} PF &= \frac{\overline{P_o}}{\overline{S}} \\ &= \frac{\overline{I}^2_{L_{rms}}}{\overline{V}_{c_{rms}} \cdot \overline{I}_{o_{rms}}} \qquad (\ p.u.), \end{aligned} \tag{3.62}$$

where $\overline{S}$ is the normalized apparent power of the tank load.

Available turn-off time With reference to equation 3.4, the available turn-off time $\overline{t_{qq}}$ is obtained as follows.

Since the phase angle of the tank load at the fundamental frequency

$$|\ \phi_1\ | = |\ \arctan[Q(\frac{\omega_s}{\omega_o} - \frac{\omega_o}{\omega_s})]\ | \qquad (\ rad\ ) \tag{3.63}$$

and

$$\phi_1 = \omega_s t_q + \frac{\pi - \delta}{2} \qquad (\ rad\ ). \tag{3.64}$$

The turn-off time is then determined by

$$\begin{aligned} t_{qq} &= \omega_s t_q \\ &= |\arctan[Q(\frac{\omega_s}{\omega_o} - \frac{\omega_o}{\omega_s})]\ | - \frac{\pi - \delta}{2} \qquad (\ rad\ ). \end{aligned} \tag{3.65}$$

The normalized turn-off time is defined as

$$\overline{t_{qq}} = \frac{1}{\pi} t_{qq} \qquad (\ p.u.\ ). \tag{3.66}$$

Evaluation format of the system responses

For all the quantities defined in the preceding paragraphs, performance curves in three different formats are considered for evaluation. These curves are the same in nature with emphasis on different parameters. They are described as follows:

1. **Outputs versus Q, with $\overline{\omega}$, p ($p = \frac{t}{\tau}$) as parameters.** This form of curves are drawn to evaluate how the system outputs vary as the load condition changes widely.

2. **Outputs versus $\overline{\omega}$, with Q, p as parameters.** The effect of variation in working frequency on the system performance is evaluated for fixed Q and p conditions; it is also referred to as the *frequency response* of the system.

3. **Outputs versus p, with ϖ, Q as parameters.** The influence of the PWM scheme on the system performance is evaluated.

It should be noted that some combinations of the parameters Q, ϖ and p may not be available because of the turn-off time limitation of PWM modulation. In this chapter, the second type, or the frequency response of the system, with selected values of p is included for discussion and later reference of the design example. Some curves of the other two types are given in Appendix B.

3.4 Description of the computer simulation of system equations

Both the computation algorithm and programming for solutions to state-space equations are of particular importance in terms of computation accuracy, speed and adaptability. Two simulation programs for the general analysis of the PWM inverter scheme proposed in the thesis are developed. The merits of each method are described briefly in this section. All other relevant description and source programs are found in Appendix A.

Runge-Kutta algorithm is commonly used because of its suitability for digital computation of higher-order differential equations, as well as its relatively high accuracy. The first simulation program adopts this algorithm. The *characteristic roots* algorithm belongs to the type of analytic method, which however requires more attention to the structure of the state equations. The program based on the second type is used as a supplementary approach to provide comparison of the simulation runs. The performance curves based on the first type of simulation results are provided and discussed in the next section.

The first simulation program using *Runge-Kutta* algorithm is written with the commercial package MATLAB, which is highly efficient in matrix operation. While the other uses both the NAG FORTRAN package and the MAPLE analytical formula solver.

The results of simulation runs have provided certain information on the computation efficiency, speed and instability problem with the two schemes. Normally, execution of programs written in MATLAB language is 1-2 times slower than those in FORTRAN running on the same machine. With the Runge-Kutta algorithm, the program runs on a VAX-8530 computer where the MATLAB software resides. The second option with the characteristic roots method uses the Dec-2000 workstation with the NAG FORTRAN package. It is found that for the solution of the same set of state equations with the same combination of parameters, running on the DEC-2000 machine achieves over at least 40 times faster speed compared with the VAX machine, in terms of CPU times. The workstation is 3-4 times faster than the VAX machine. This is due mostly to the nature of operation. The analytical scheme contains mainly simpler operations as a result of using MAPLE package. The ease of programming, however, is quite different. With the *Runge-Kutta* scheme, a general-purpose simulation program can be developed, which may suit many systems of different configurat:.ns. The program based on the *characteristic roots* method is, however, very suitable for solving a fixed set of state equations, as the major efforts are very much dependent on the system structure, which determines the formulation of the equations.

3.5 Simulation results

The results produced by MATLAB programs according to the format mentioned in section 3.3.5 are taken for example and discussion. Performance curves based on the second type of format, the *frequency response*, are shown in Figure 3.8 - 3.13 at the end of this chapter. All the curves in other formats are provided in Appendix B for further reference. The performance curves presented in Figure 3.8 to 3.13 are drawn with $\overline{\omega}$, the normalized frequency, as the self variable and Q, p as parameters. For each pair of figures, three curves representing different Q values are plotted, with a particular value of p. Specifically, the figure with p as 1.0 actually corresponds to the non-PWM scheme. The average choke current $I_{d_{ave}}$, RMS coil current $I_{L_{rms}}$, RMS output current $I_{o_{rms}}$, effective output power P_o, RMS and maximum output voltages $V_{c_{rms}}$, $V_{c_{max}}$, tank power factor PF and available turn-off time t_q are provided, all in the normalized form.

3.5.1 Discussion on the system performance

1. " **Peak phenomenon:**"

   It is noticed in most of the current and voltage curves, a peak value is identified for each particular curve. This peak occurs with $\overline{\omega}$ at around 1.1. Due to the inherent characteristics of the current source used in the CSI inverter, the steady-state value of the source will not be unique for different system parameters unless some means is provided. Normally a controlled rectifier together with a closed-loop current control is used to maintain the current constant. With the PWM CSI scheme, a diode rectifier is employed, instead. It is seen in the curves of $I_{d_{ave}}$ that this current has quite different values under different Q. The operating frequency also has an influence on the current, especially when it is close to the resonant frequency, ω_o, of the load. The output power, which is related to the output current, is not so high at frequencies very close to ω_o, because better tuned load possesses a very high impedance so that the DC link current is low, with a constant voltage source. On the other hand, the DC link current reaches a higher value when ω_s is far away from ω_o, but the resultant output is lower because of the large degree of detuning. That is why the peak is observed. For very low Q values, such as Q_o=2, however, it is not significant. This property indicates that to achieve a designated output, the working frequency is not necessarily set closest to ω_o, as with the conventional inverters. The peak should be avoided, as this may result in too high a coil voltage, which increases the component ratings. The PWM index, p, has similar effect on the component stress. This is illustrated in the figures included in Appendix B.

2. **DC link current:**

In addition to the operating frequency ω_s and parameter Q, p also affects this current around the " peak " frequency. That is, when p decreases, $I_{d_{ave}}$ increases, and the output power also increases. It is different from the case of a PWM VSI inverter, which is on the contrary. This is again because the DC link current is not constant under different parameters. In any case, the PWM scheme can affect this current, and therefore the output power.

3. **Output voltage:**

The output voltage, or the compensating capacitor voltage, increases substantially with an ascending order of Q values. With high Q values, both ϖ and p have an obvious effect on the voltage. This should be taken into consideration in the design of the inverter.

4. **The output current and power:**

   Both normalized quantities are related to a base which is Q dependent, so the actual values of these quantities with different Q values should be found in terms of the base. The tendency of the change of the quantities with a particular Q, however, shows directly the relative amount. These changes are compatible with the discussion above.

5. **Tank power factor:**

   The figures shows the following facts:

   - lower ϖ ensures a higher PF;
   - p has little influence on PF, once equation 3.4 is satisfied. This property is twofold: it is useful because with ϖ fixed, the output power can be adjusted within a range of p without affecting PF too much, while it might be different if only swept-frequency scheme is available. On the other hand, this condition is more difficult to meet compared with the non-PWM scheme, as can be seen from Figure 3.3 and 3.4.

6. **Turn-off time**

   The curves also show that:

- higher Q enables a higher turn-off time, so the case of lowest Q provides the smallest t_q;
- higher $\overline{\omega}$ ensures a higher t_q, while the performance of the system would be poorer, if it is too high;
- t_q is linearly related to p; higher p gives a high t_q (see figures in Appendix B). Referring to equation 3.4 again, with fixed ϕ at certain Q, $\omega_s t_q$ is directly proportional to δ. This means that if the available turn-off time is determined to be larger than t_{off}, the operating frequency is limited by the δ. Or ϕ in this case increases if ω_s is not low, but this affects PF.

  This can also be observed with the help of the curves. For $p < 1$, the condition of the PWM scheme is not satisfied with lower $\overline{\omega}$, especially when Q is small.

From the discussions above, the PWM CSI inverter is able to regulate the output power by both the swept-frequency method and the PWM scheme. The working frequency of the inverter should not be too close to the resonant frequency of the load, and this is also beneficial to the available turn-off characteristics of the inverter. The peak phenomenon, however, should be avoided. If $\overline{\omega}_s$ is too large, the power factor will be poor and output low. A compromise should be made, especially when the Q range of the load of the inverter to be designed is very wide.

3.5.2 Simulation waveforms

The waveforms of the simulation results of $\overline{i_d}$, $\overline{i_L}$, $\overline{v_C}$ and $\overline{i_o}$, with normalized parameters $\overline{\omega} = 1.10$, $Q = 2$, and $p = 0.8$ are presented in Figure 3.7. It is seen that the choke current i_d is almost constant over the time axis. The difference in value within half a period of the switching frequency, because of the charging/discharging effect of the choke, can be totally neglected. Both the tank voltage and coil current have a nearly sinusoidal wave-shape, even though Q is not high. The waveform of i_o shows that the PWM scheme is in effect. The amplitude of this current is very close to that of the DC line current.

Some experimental verifications of the simulation results are provided in Chapter 4, together with a design example.

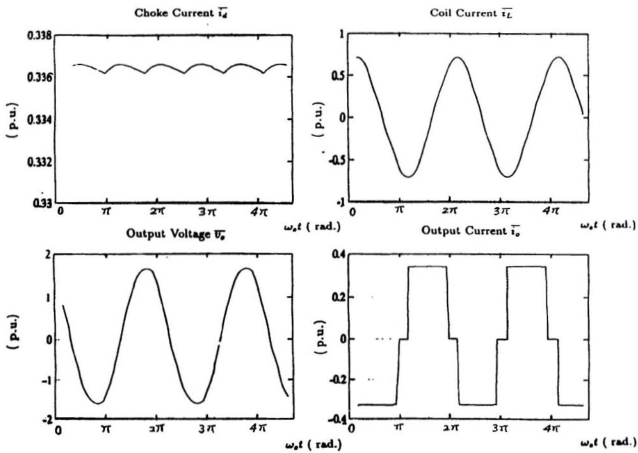

Figure 3.7: Simulation waveforms of $\overline{i_d}$, $\overline{i_L}$, $\overline{v_c}$ and $\overline{i_o}$, at $\overline{\omega} = 1.10$, $Q_o = 2$, and $p = 0.8$.

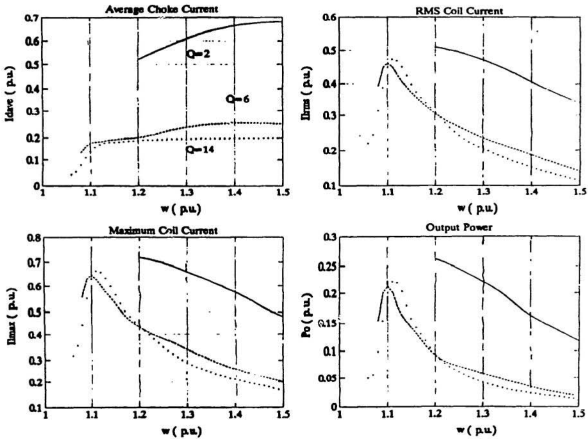

Figure 3.8: Simulation results: Frequency Response of $\overline{I_{dave}}$, $\overline{I_{Lrms}}$, $\overline{I_{Lmax}}$ and $\overline{P_o}$ with $p = 0.6$.

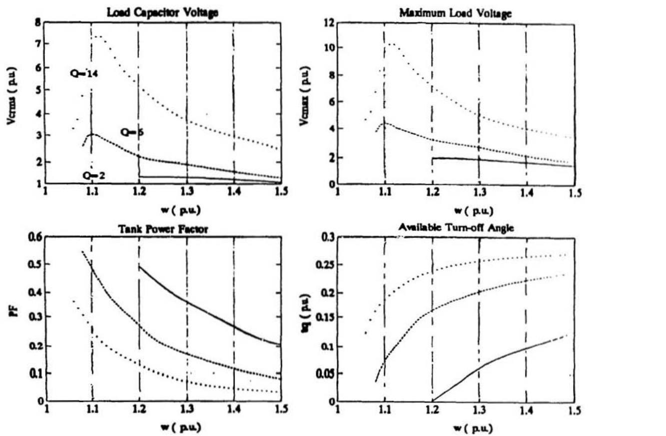

Figure 3.9: Simulation results: Frequency Response of $\overline{V_{crms}}$, $\overline{V_{cmax}}$, PF and $\overline{t_{qq}}$ with $p = 0.6$.

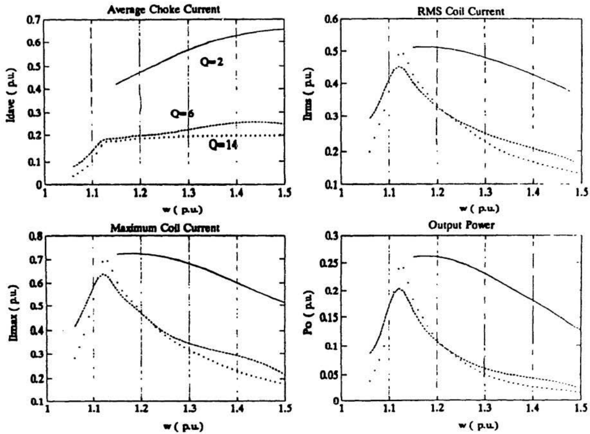

Figure 3.10: Simulation results: Frequency Response of $\overline{I_{dave}}$, $\overline{I_{Lrms}}$, $\overline{I_{Lmax}}$ and $\overline{P_o}$ with $p = 0.7$.

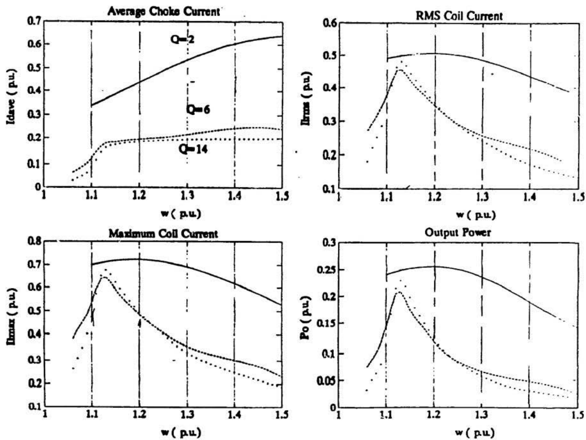

Figure 3.12: Simulation results: Frequency Response of $\overline{I_{dave}}$, $\overline{I_{Lrms}}$, $\overline{I_{Lmax}}$ and $\overline{P}_o$ with $p = 0.8$.

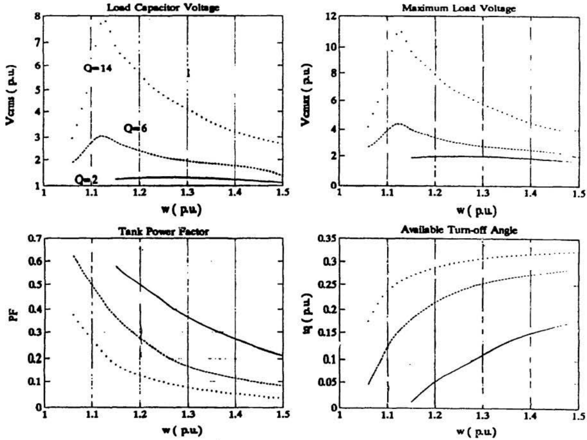

Figure 3.11: Simulation results: Frequency Response of $\overline{V_{crms}}$, $\overline{V_{cmax}}$, PF and $\overline{t_{qq}}$ with $p = 0.7$.

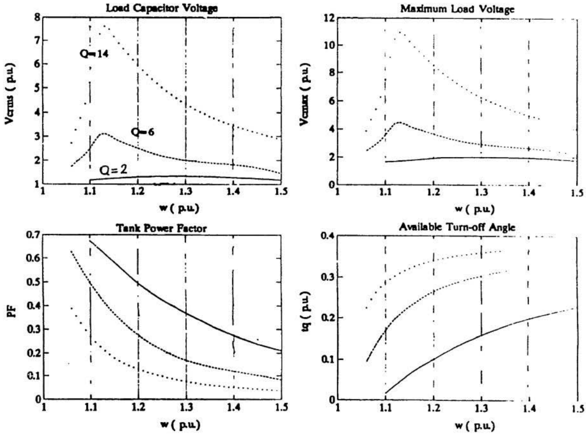

Figure 3.13: Simulation results: Frequency Response of $\overline{V_{crms}}$, $\overline{V_{cmax}}$, PF and $\overline{t_{qq}}$ with $p = 0.8$.

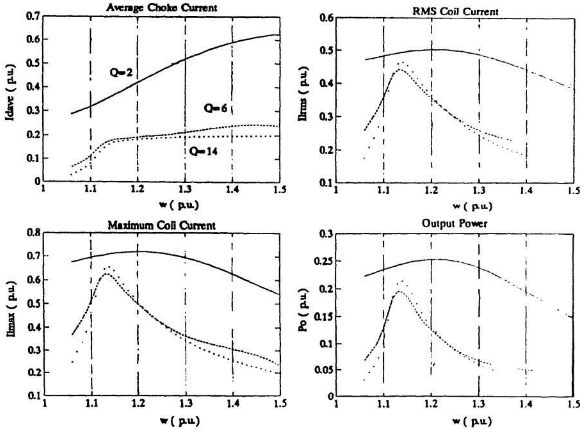

Figure 3.14: Simulation results: Frequency Response of $\overline{I_{dave}}$, $\overline{I_{Lrms}}$, $\overline{I_{Lmax}}$ and $\overline{P}_o$ with $p = 0.9$.

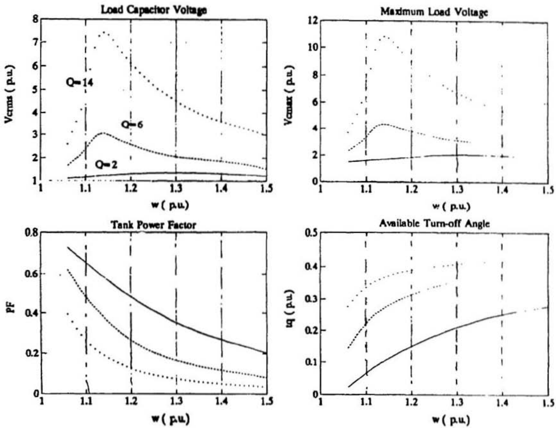

Figure 3.15: Simulation results: Frequency Response of $\overline{V_{crms}}$, $\overline{V_{cmax}}$, PF and $\overline{t_{qq}}$ with $p = 0.9$.

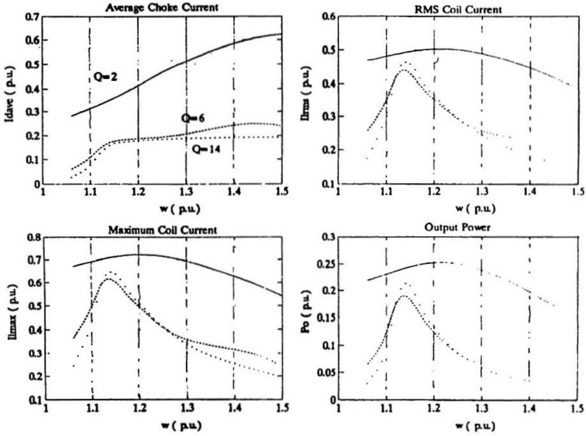

Figure 3.16: Simulation results: Frequency Response of $\overline{I_{dave}}$, $\overline{I_{Lrms}}$, $\overline{I_{Lmax}}$ and $\overline{P_o}$ with $p = 1.0$.

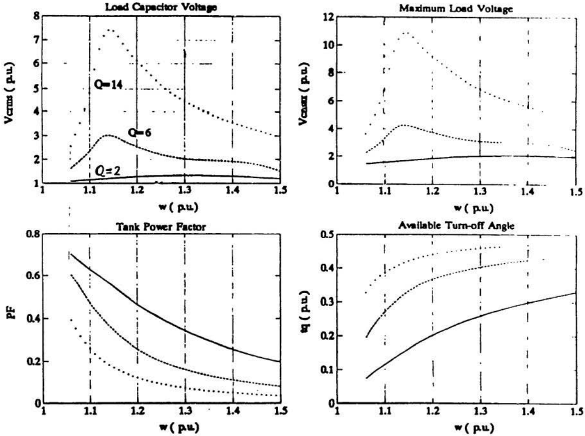

Figure 3.17: Simulation results: Frequency Response of $\overline{V_{crms}}$, $\overline{V_{cmax}}$, PF and $\overline{t_{qq}}$ with $p = 1.0$.

Chapter 4

Design and Implementation of the PWM CSI System

The design and implementation of the PWM CSI system presented in this thesis are divided into two major parts: the PWM triggering circuit which is used to realize the PWM scheme in the inverter system, and the inverter system including the DC link, inverter bridge and the tank load. Both specifications and realization of these two parts are provided in this chapter, with a design example showing the procedure how to use the performance curves obtained in Chapter 3 for the design of the inverter system. Experimental verifications are supplied, which show the satisfactory agreements between theoretical and laboratory results.

4.1 Realization of the PWM triggering circuit

Triggering circuits can be realized by either hardware or software means. Hardware implementation may provide smaller sizes and lower cost, compared to those by software method where a computer or a microprocessor is involved. The advantage of using a computer is that, in addition to allowing complex control algorithms, the triggering signals can be obtained easily by programming a timer. For many induction heating applications, the control and the triggering circuitry may be achieved by hardware implementation, because the control requirements are relatively simple. The triggering circuit implemented in this thesis is an all-IC circuit which is simple and provides the required pulses in agreement with the proposed scheme.

4.1.1 Working principle and requirements of the PWM triggering circuit

Common requirements of a triggering circuit for thyristor inverters are listed below [19].

1. All the pulses should have a reasonable voltage level, such as $5\,Volts$ from the output of TTL circuits, to be coupled to the pulse amplifier, with a duration no less than $20\,\mu s$ for reliable triggering. Too wide a duration would saturate the pulse transformer. Where the precise pulse width cannot be ensured, the usual alternative is to modulate the wider pulses with a $30\,kH_z$ square wave of about 33% duty ratio.

2. The number of individual triggering signals for different thyristors is determined by the demand of particular power circuits. The signals may have some relative phase differences with one another, but should all be synchronized to the main pulse generator. The sequence of the pulses is controlled by other circuits.

3. Within the designated range of working frequencies, the amplitude of the triggering pulses should remain constant. Where PWM schemes are required, continuous phase shifting capability is to be ensured.

4. For the purpose of closed-loop control, together with other control circuits, the triggering circuit is supposed to have voltage-controlled characteristics, so that both A/D and D/A converters can be interfaced.

The operation of the triggering circuit for the particular inverter in this thesis can be divided into two basic parts: the starting process and the steady-state process. In the first case, the main task of the circuit is to successfully initialize the CSI inverter system from a "cold" state. The PWM pattern may not be a major concern during this transient period. After the inverter reaches its normal operation, the PWM scheme is then used to regulate the output, as described in Chapter 3.

In Figure 3.1, the function of T_5 and T_6 is to help build up the initial current in the choke and voltage in the tank used for the load commutation so that the inverter can be started from cold. This starting circuit adopts the type of circuit introduced in the literature [1].

Referring to Figure 3.1 and 3.4 of Chapter 3, it is seen that for the thyristors in the bridge composed of T_1 to T_4, in the steady-state, individual triggering is required for this PWM inverter. Besides, the theoretical phase shift is supposed to range from 0 to π rad., with the resultant output current from its maximum to zero.

Figure 4.1 shows the circuit diagram and relevant waveforms of the triggering circuit. In realizing the practical circuit, three modes of the operation are considered. In mode 1, only T_1 and T_6 are involved to establish the DC current in the choke. The operation of mode 2 is to alternatively switch thyristor pairs T_2, T_5 and T_3, T_6, which just last for a few cycles until a sufficient voltage is established across the tank circuit. After that, mode 3

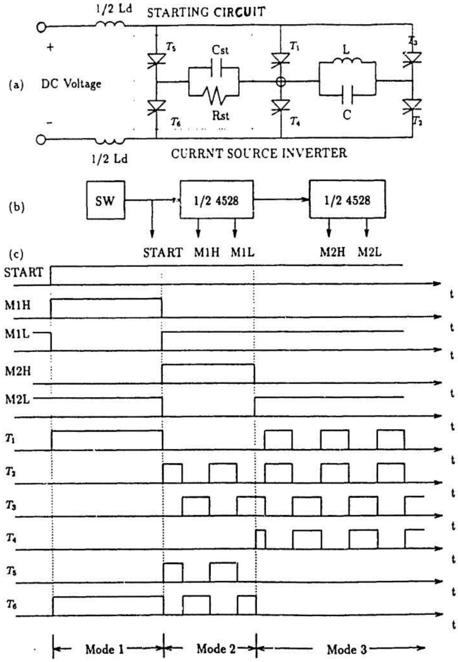

Figure 4.1: Starting circuit, mode control diagram and relevant waveformes.

begins with only the thyristors in the bridge being active. As to the triggering circuit, the actual triggering throughout all the three modes is controlled with the help of mode control circuit, as illustrated in Figure 4.1 (b). Auxiliary triggering signals used for the operation are designated as START, M1H, M1L, M2H and M2L. Take M1H for example, which means " high " level during mode 1.

All the triggering signals are coupled to the thyristors of the inverter through a *driver circuit* and a *pulse transformer* [19].

4.1.2 Implementation and specifications of the PWM triggering circuit

The block diagram of the triggering circuit is given in Figure 4.2, which is considered for the requirements introduced in the last section. In the circuit, V_M is used to adjust the phase shift range, while E_o is the voltage to control the frequency of the output signals. The final signals are of a width of $20\mu s$ without the $30kHz$ modulation waveforms.

For the closed-loop control operation, both V_M and E_o can be interfaced with A/D or D/A converters through some auxiliary circuits. Besides, the phase angle shift range covers from 0 to 0.7π rad., which corresponds to the δ range of 0.3π to π. This is because for the application of the PWM scheme to CSI circuits, δ lower than 0.5π is less meaningful.

The main specifications for the triggering circuit used for the laboratory verification are listed in Table 4.1. The design and implementation of the specific circuits along with theoretical/experimental waveforms are included in Appendix C.

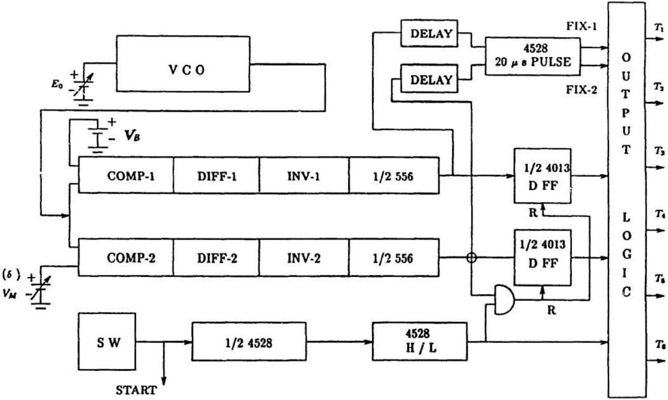

Figure 4.2: Block diagram of the triggering circuit.

Table 4.1: **Specifications of the triggering circuit**

DC Supply Vcc:	10	to	12 Volts
V_M adjust range:	3.2	to	6.7 Volts
Phase shift range:	0	to	0.7π
E_0 adjust range:	0	to	20 Volts
Frequency range:	330	to	1600 Hz
Output voltage level:	10 Volts (CMOS)		

4.2 Experimental set-up and verifications of the PWM CSI inverter

In this section the specifications for the major components used in the experimental set-up are briefly introduced, followed by a design example which illustrates the use of the normalized performance curves to determine the working parameters as well as the ratings of components. Experimental verifications of the simulation results are presented. Since the PWM scheme is used for the purpose of output power regulation, an output power regulation test is conducted to verify the scheme and the results are compared with the theoretical values.

4.2.1 Experimental set-up for verification of simulation results

Current source inverters normally work at power levels up to hundreds of kilowatts. Substantially high current and voltage are observed. However, prototype laboratory set-up with power level of 100 watts is used to obtain the experimental results. The circuit diagram of the system in the experiment is given in Figure 4.3, which is actually identical

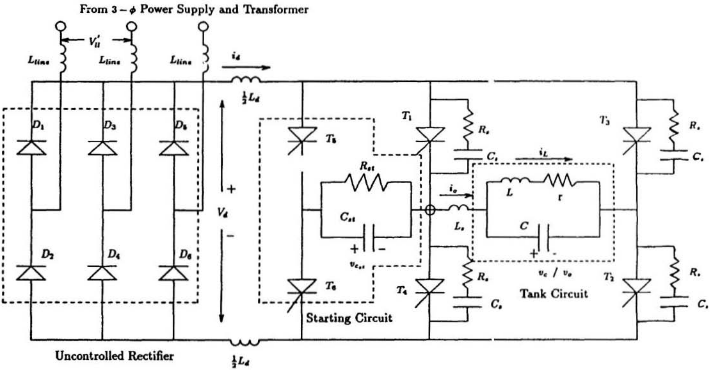

Figure 4.3: Experimental set-up of the proposed PWM inverter.

Table 4.2: **Specifications of the experimental circuit**

AC supply source:	$V_{ll} = 208V$
	Line frequency $f_i = 60\ Hz$
D_1 to D_6:	Power diodes (R410-1240)
Line inductors:	$L_{line} = 20\ mH$
Smoothing inductor:	$L_d = 2.0\ H$
Inverter bridge:	Three phase current source inverter
	T_1 to T_6: 36RC80A-8013 ($t_{off} = 30\ \mu s$)
Load circuit:	$L = 4.45\ mH$; $C = 9\ \mu F$;
	$r = 1.33 - 12\Omega$ ($Q = 2 - 18$)
	Resonant frequency: $f_o \doteq 850\ Hz$

to Figure 3.1. The values of major components used in the experimental set-up and other specifications are listed in Table 4.2.

In the test, V_{ll}' is selected as 45 $Volts$, so E equals to 60 $Volts$. The power level used for the regulation is set to 60 $Watts$.

4.2.2 Design example of the PWM inverter

In the design of conventional non-PWM CSI inverters, regulation of the output power is the task of the controlled rectifier. Therefore the working frequency is normally set close to the resonant frequency of the load circuit.

In the system proposed in this thesis, because of the use of PWM technique, parameters like p and ω are considered concurrently with the variation in Q values, in order to realize the power adjustment. To illustrate the basic functions of this system, an assumption is made that variation in Q values is due only to changes in the equivalent resistance, r. It should be noted, however, that under this condition, the normalization bases also change with Q, which is to be considered in the design.

A design example is provided, which considers the extreme case when Q varies from 2 to 18. This variation can actually cover the range of any practical induction heating load.

Design example:

A combination of parameters is needed for the regulation of the output power under wide variation in Q values. Firstly the normalized power values which correspond to respective Q values should be found under constant power assumption. Secondly, the combination of parameters ω and p in each case is selected from the performance curves presented in Chapter 3, satisfying the normalized power values found in the first step. Finally, given specific requirements, ratings of the major components are determined according to the above results.

With constant output power P_o and input voltage V'_{II}, for different Q_o values, the relationship between normalized power, $\overline{P}_o$, and Q_o is given by

$$P_B = \frac{E^2}{r} \tag{4.1}$$

$$Q_o = \frac{\omega_o L}{r} \tag{4.2}$$

$$\overline{P}_o = \frac{P_o}{P_B} \tag{4.3}$$

Table 4.3: **Relationship of Q_o and $\overline{P_o}$ under the constant power assumption.**

$\mathbf{Q_o}$	2	6	10	14	18
$\overline{\mathbf{P_o}}$	$\overline{P}_{oQ_o=2}$	$\frac{1}{3}\overline{P}_{oQ_o=2}$	$\frac{1}{5}\overline{P}_{oQ_o=2}$	$\frac{1}{7}\overline{P}_{oQ_o=2}$	$\frac{1}{9}\overline{P}_{oQ_o=2}$

$$\frac{\overline{P}_{o_1}}{\overline{P}_{o_2}} = \frac{Q_{o_2}}{Q_{o_1}} \tag{4.4}$$

For the Q values of 2, 6, 10, 14 and 18, and with $\overline{P}_{Q_o=2}$ as the base, the respective normalized power values are given in Table 4.3.

Respective ω and p values can be determined with the help of corresponding performance curves, the frequency response curves in Chapter 3. Since the absolute value of $\overline{P}_{oQ_o=2}$ is the largest, it should be selected properly so that the others can be chosen without difficulty. There may be many options to choose the combination, while the basic rule is that they should be decided with the overall performance as satisfactory as possible. In addition, the important thing is to find a region where close ratios of different normalized power levels with different Q values could be obtained.

Choose $\overline{P}_{oQ_o=2}$ as 0.25, for example, at $\overline{\omega} = 1.27$ and $p = 0.7$ in Figure 3.10. The resultant normalized power values at other Q values are found according to Table 4.3. In addition, values of all other variables in normalized form are also determined with the frequency response curves. The results are listed in Table 4.4.

In this design of the inverter the following specifications are given:

Power supply: $3-\phi$ AC supply at $60H_z$;

Table 4.4: **Normalized output values with $\overline{P_o}(Q_o = 2) = 0.25$ $(p.u.)$.**

Q_o	$\overline{\omega}$	$p(\delta)$	$\overline{P_o}$	$\overline{I_d}$	$\overline{I_L}$	$\overline{I_o}$	$\overline{V_c}$	PF	$\overline{t_{qq}}$
2	1.27	0.7	0.25	0.6	0.47	0.48	1.13	0.36	0.04
6	1.08	1.0	0.083	0.09	0.3	0.08	2.0	0.5	0.21
10	1.07	0.7	0.05	0.055	0.24	0.048	2.6	0.47	0.08
14	1.06	0.6	0.036	0.048	0.22	0.035	3.2	0.37	0.13
18	1.06	0.9	0.028	0.028	0.17	0.03	3.1	0.32	0.31

Resonant frequency: $f_o = 400 \;\; Hz$;

Rated output power: $P_o = 10$ kW;

Load parameters: $L = 1 \;\; mH$ and $Q_o = 2 - 18$;

Device turn-off time: $t_{off} = 20 \;\; \mu s$.

Since all the parameters are selected based on the constant power assumption, the required input voltage can actually be determined in terms of any Q value. Take $Q_o = 2$ as reference, and the equivalent resistance is $r = \frac{\omega_o L}{Q_o} = \frac{2 \times \pi \times 400 \times 10^{-3}}{2} = 1.26\, ohms$. The input line to line voltage can then be decided, referring to Table 4.4, by

$$
\begin{aligned}
E &= \sqrt{P_B \times r} \\
&= \sqrt{\frac{P_o}{\overline{P_o}} \times r} \\
&= \sqrt{\frac{100 \times 10^3}{0.25} \times 1.26} \\
&\doteq 225 \;\; Volts;
\end{aligned}
$$

$$
\begin{aligned}
V'_{ll} &= \frac{1}{1.35}E \\
&\doteq 166\ Volts.
\end{aligned}
$$

$E = 1.35V'_{ll}$ is then selected as the base so $V_B = 225\ Volts$ (1 p.u.). The thyristor ratings are decided as follows.

The maximum thyristor voltage $\hat{V}_{AK}$ occurred at $Q_{o_{max}} = 18$ is equal to the maximum load voltage v_c. The corresponding maximum normalized load voltage $\overline{v_{c_{max}}}$ is 3.1 (p.u.), therefore,

$$
\begin{aligned}
\hat{V}_{AK} &= \sqrt{2} \times 3.1 \times 225 \\
&\doteq 986\ Volts. \qquad (4.5)
\end{aligned}
$$

The RMS value of the thyristor current is directly proportional to the RMS output current. The maximum value of the output current occurs at $Q_o = 2$, where $\overline{I_o} = 0.48$ $(p.u.)$.

$$
\begin{aligned}
I_Q &= \frac{1}{\sqrt{2}}I_o \\
&= \frac{1}{\sqrt{2}}I_B \times \overline{I_o} \\
&= 0.707 \times \frac{225}{1.25} \times 0.48 \\
&\doteq 61\ Amps. \qquad (4.6)
\end{aligned}
$$

To limit the short-circuited current of the system, L_{line} is determined as follows. In this situation, because of the symmetrical structure of the 3 ϕ source, the maximum current is selected according to I_Q, and can be found easily with one phase and L_{line} is determined.

$$
\begin{aligned}
I_Q &= \frac{V_{ll}'}{\sqrt{3} \times \omega_i L_{line}}, \qquad (4.7)\\
L_{line} &= \frac{V_{ll}'}{\sqrt{3}\omega_i I_Q}\\
&= \frac{225}{2 \times \pi \times f_i \times I_Q}\\
&= \frac{166}{2 \times \sqrt{3} \times \pi \times 60 \times 61}\\
&\doteq 4.17\ mH. \qquad (4.8)
\end{aligned}
$$

Choose L_{line} as 5 mH. Since $\frac{L_d}{L_{line}} \geq 100$, as considered in the simulation, L_d is selected as 1 H.

The value of the compensating capacitor is

$$
\begin{aligned}
C &= \frac{1}{\omega_o{}^2 L}\\
&= \frac{1}{2 \times \pi \times 400^2 \times 10^{-3}}\\
&= 157\ \mu F, \qquad (4.9)
\end{aligned}
$$

and the maximum capacitor voltage, $V_{c_{max}}$, is the same as that of the thyristors, i.e., $V_{c_{max}} = 986\ Volts$. Since v_c is basically close to sinusoidal, the RMS capacitor current can be found as:

$$
I_{c_{rms}} = \frac{1}{\sqrt{2}} \frac{V_{c_{max}}}{\frac{1}{\omega_s C}}
$$

$$= 0.707 \times 986 \times 1.27 \times 2 \times \pi \times 400 \times 157 \times 10^{-6}$$

$$\doteq 350 \ Amps. \tag{4.10}$$

From Table 4.4, the lowest normalized available turn-off angle, when Q_o equals to 2 and $\overline{\omega_s}$ equals to 1.27 (p.u.), is 0.04 (p.u.). Therefore the actual minimum turn-off time is given by

$$\begin{aligned} t_q &= \frac{\pi \times \overline{t_{1q}}}{\omega_s} \\ &= \frac{0.04 \times \pi}{1.27 \times 2 \times \pi \times 400} \\ &\doteq 39.4 \ \mu s. \end{aligned} \tag{4.11}$$

This example is provided to give a brief description of how to design and estimate the system under specific conditions. With the components selected above, the system can deliver the rated power to the load at a range of Q_o from 2 to 18, keeping the components within safe limits. It is obvious that the performance of the system covering a wide range of Q is more difficult to design, especially at low Q values.

4.2.3 Experimental verification

The simulation results as selected in Table 4.4 are experimentally verified with Q_o from 2 to 14. The power level used in the test is 60 $Watts$, and $E = 60 \ Volts$ ($V'_{ll} \doteq 45 \ Volts$, as given in subsection 4.2.1). Both the measured values and the simulated ones that are in the actual units, converted from the normalized form in Table 4.4, are shown in Table 4.5. It is seen from Table 4.5 that the experimental results are close to the theoretical values.

Table 4.5: **Experimental verification of Table 4.4.**

Q_o	$\overline{\omega_s}$	$p(\delta)$	$P_o(W)$	$I_d(A)$	$I_L(A)$	$I_o(A)$	$V_c(V)$	PF
2	1.27/1.27	0.7/0.7	60/60	3.0/3.3	2.35/2.2	2.4/2.7	67.8/75	0.36/0.3
6	1.08/1.08	1.0/0.9	60/60	1.35/1.7	4.5/4	1.2/1.3	120/115	0.5/0.4
10	1.07/1.07	0.8/0.8	60/60	1.38/1.5	6.0/5.0	1.2/0.99	156/134	0.47/0.46
14	1.06/1.06	0.9/1.0	60/60	1.68/1.6	7.7/6.5	1.22/0.9	192/176	0.37/0.4

* Left: simulation results; right: experimental results.

The errors, which are within the acceptable range, can be subject to factors such as reading of the measurements meters, conversions of different units, accuracy of the components values, particularly the values of the inductance, as well as the possible minor numerical error in the calculation of the state equations.

Some selected waveforms of i_d, i_L, v_c and i_o are presented in Figure 4.4, for the verification of Figure 3.7 in Chapter 3, and Figure 4.5 for that in Table 4.5. Corresponding to Figure 4.4, the predicted values versus those in the normalized form in Figure 3.7 are: $I_L = 2.47\,A$, $V_c = 72\,V$ and $I_o = 3.4A$, respectively.

All the currents and voltages, such as I_L and V_c, given in the tables and figures are RMS values.

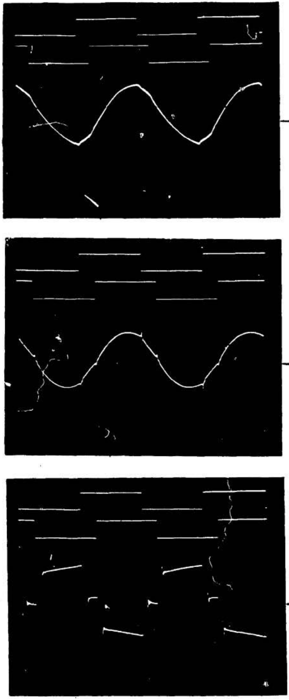

i_L — 0

X: 0.24 ms/div.

Y: 3 A/div.

H: 10 divs

V: 8 divs

v_c — 0

X: 0.24 ms/div.

Y: 90 V/div.

i_o — 0

X: 0.24 ms/div.

Y: 1.5 A/div.

Figure 4.4: Experimental verification of the inverter steady state responses of Figure 3.7 $Q_o = 2$, $f_s = 940\,H_z$, $f_o = 850\,H_z$ ($\overline{\omega} = 1.10$) and $p = 0.8$. All upper curves: indication of phase shift due to PWM.

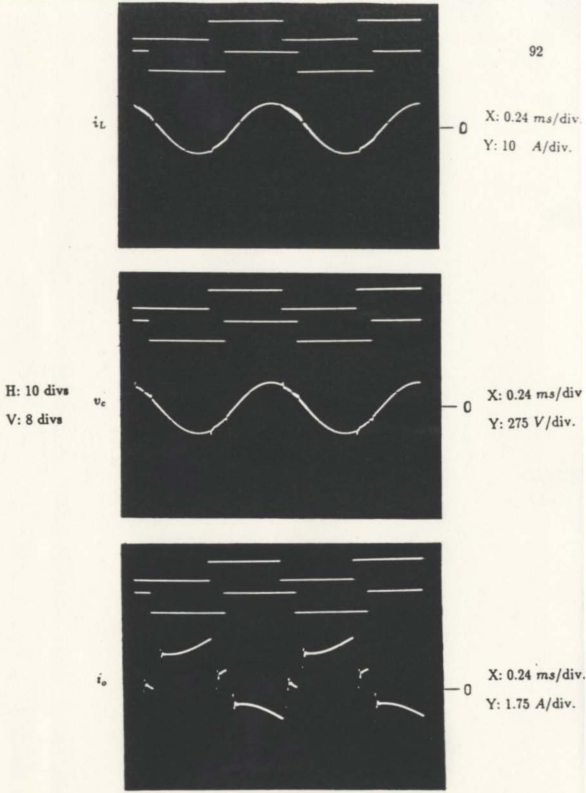

Figure 4.5: Experimental verification of the steady state responses of Table 4.5: $Q_o = 10, f_s = 900\,H_z,\ f_o = 850\,H_z$ ($\overline{\omega} = 1.06$) and $p = 0.8$. All upper curves: indication of phase shift due to PWM.

Chapter 5

Conclusions

In this thesis the development and implementation of a PWM CSI inverter are presented. The analytical results, verified by the experimental data, show the feasibility of the scheme. With this scheme, a simple and low-cost system can be developed that provides the same functions as are available with a conventional CSI inverter.

Extensive simulation has been conducted to achieve various steady-state responses that are used to fully describe the system performance. The following characteristics are found regarding the system behaviour.

1. The " constant " DC current source realized in the inverter has different values with different combination of parameters, such as $\overline{\omega}$, Q and p. This fact results in the " peak " response phenomenon. It is basically different from a conventional inverter in that the working frequency is set to a value which is not very close to the resonant frequency of the induction heating load.

2. Due to the effect of the PWM scheme, the system responses change differently from a conventional system. For instance, sometimes narrower pulses in the out-

put waveform correspond to a higher RMS output, because the amplitude of the output current could be larger than that with a full output waveform. The potential meaning of the PWM scheme in this inverter is that the scheme can complete the output power regulation task together with the swept-frequency method; no additional control effort is needed.

3. The power regulation over a wide range of Q, from 2 to 18, can be achieved. At certain Q values, the tank power factor is lower than that of a non-PWM CSI inverter. On the average, the performance is satisfactory.

4. The PWM scheme results in a little more stress on the components than a conventional inverter. The design should therefore be based on the ratings under the worst case.

5. With the PWM scheme applied to the inverter bridge, the controlled rectifier is eliminated. This permits a simpler design of the closed-loop current control. In order to provide a protection means to the inverter, which is achieved by the controlled rectifier in a conventional inverter, line inductors are intentionally introduced in the input lines of the PWM CSI inverter. It is a simple method without affecting the system performance. In addition, this inductance also functions as a filter which improves the wave-shape of the input line current/voltage so that less negative effect due to the regulation of the inverter is reflected to the utility line.

The power regulation test conducted in the laboratory verified the theoretical results and the experiment data reflected the phenomenon discussed above.

The design and implementation of a PWM triggering circuit is one of the key parts to ensuring the successful operation of the PWM CSI inverter. This circuit is achieved by hardware means, and is simple and reliable. It can be further integrated with the VLSI technique. The A/D and D/A interfacing for the closed-loop control task can be done with the help of a few more auxiliary circuits .

The simulation results show that with one more major parameter, p, the numerical analysis is more difficult to conduct. Larger amount of computation is demanded, in which case the simulation method, or the computation algorithm, is of particular importance. The results obtained in this thesis are based on a third-order dynamic system equation set. The second method adopted in the analysis, which is mainly for the comparison of the computation speed, can be a better choice if the configuarion of the system to be simulated is relatively fixed.

The contribution of this thesis is that the characteristics of the proposed current source inverter under PWM scheme are investigated. The system behaviour has thoroughly been discussed based on the analysis and description of the operation principles, simulation results and the experimental verifications. In addition, the research also provides a means of reference for the design of a practical system.

Suggestions

The research work presented in this thesis is conducted for a PWM CSI inverter other than the conventional ones, while the basic configuration is used in order not to divert the attention from obtaining the major characteristics of the scheme. A slightly more

Complex configuration, such as that with a series-parallel load, may be of interest in order to enhance some functions of the system. Further evaluation is needed in this case as the system equation set tends to be of fourth-order. Besides, further investigation should be conducted in cases when not only Q, but also the resonant frequency of the tank load vary. In any case, a highly efficient simulator is necessary for a successful evaluation of the system performance. Further discussion on this issue may be desired.

From the closed-loop control point of view, a carefully designed control strategy is to be proposed, with more parameters to be considered at the same time. In addition, how to effectively sense the change of Q values, as well as any other variations will be also a major task. In realizing the control scheme, probably a look-up table would be essential and favourable, since the combination of many parameters to be ensured for successful regulation of the output power is of a multi-optional nature.

References

[1] B. R. Pelly, " Latest Developments in Static High Frequency Power Sources for Induction Heating ", IEEE Trans. on Ind. Electron., Vol. IECI-17, no.4, June, 1970, pp.297-312

[2] P. Dawson and P.K. Jain, " A Comparison of Load Commutated Inverter Systems for Induction Heating and Melting Applications ", IEEE Trans. on Power Electron., Vol.6, no.3, July, 1991, pp.430-441

[3] K. B. Zhao and P. C. Sen, " A Thyristor Inverter for Medium-Frequency Induction Heating ", IEEE Trans. on Ind. Electron. Vol. IE-31, no.1, February, 1984, pp.34-36

[4] J. Davies and P. Simpson, *Induction Heating Handbook*, McGRAW-HILL Book Company (UK) Limited, 1979

[5] P. K. Jain, " A Clamped Series Inverter for Induction Heating ", Master's Thesis, University of Toronto, 1984

[6] F. Brichant, *Forced-Commutated Inverters*, North Oxford Academic Publishing Company Limited, Oxford, England, 1984

[7] G. F. Bobart, " High Frequency Solid State Power -- Key to Process Performance ", *Induction Heating*, Vol. 56, no. 6, June, 1989, pp.22-26

[8] G. Ledwich, " Current Source Inverter Modulation ", IEEE Trans. on Power Electron., Vol. 6, no.4, October, 1991, pp.618-623

[9] G. Joos, G. Moschopoulos, and P.D. Ziogas, " A High Performance Current Source Inverter ", in Conf. Record IEEE PESC, 1991, pp.123-130

[10] P.N. Enjeti, P.D. Ziogas and J.F. Lindsay, " A Current Source PWM Inverter with instantaneous Current Control Capability ", IEEE Trans. on Ind. Appli., Vol.27, no.3, May/June, 1991, pp.582-588

[11] J. E. Quaicoe, " Analysis and Design of A 6-Pulse Cyclo-inverter", Ph.D Thesis, University of Toronto, 1981

[12] S. B. Dewan and G. Havas, " A Solid-State Supply for Induction Heating and Melting ", IEEE Trans. on Ind. and Gen. Applications, Vol. IGA-5, no.6, Nov./Dec. 1969

[13] G. N. Revankar and S. A. Gadag, " Analysis of High-Frequency Bridge Inverter Circuit ", IEEE Trans. on Ind. Electron., Vol. IECI-20, no.3, August, 1973, pp.178-182

[14] G. N. Revankar and S. A. Gadag, " A High-frequency Bridge Inverter with Series-Parallel Compensated Load " , IEEE Trans. on Ind. Electron., Vol. IECI-21, no.3, no.1, February, 1974, pp.18-21

[15] M. R. Roda and G. N. Renvankar , " Voltage-Fed Discontinuous Current Mode High-Frequency Inverter for Induction Heating ", IEEE Trans. on Ind. Electron., Vol.IECI-25, no.3, August, 1978, pp.226-232

[16] M. H. Rashid, *Power Electronics*, Prentice Hall, Englewood Cliffs, NJ, 1988

[17] N. Mohan, T. M. Undeland and W. P. Pobbins, *Power Electronics*, John Wiley & Sons, 1989

[18] W. H. Press, *et al*, *Numerical Recipes*, Cambridge University Press, 1989

[19] G. K. Dubey , S. R. Doradla , A. Joshi and R. M. K. Sinha, *Thyristorised Power Controllers* , John Wiley & Sons, 1986

[20] R. Yorke, *Electric Circuit Theory*, Pergamon Press, 1986, pp. 177-179

Appendix A

Description of the Simulation Programs

A.1 Simulation program 1 in MATLAB based on Runge-Kutta algorithm

The flow chart of simulation run is given in Figure A.1. Three major loops are used for p, Q_o and $\overline{\omega}$. Different choices of variables for horizontal axis in the graphs result in curves in three different formats. Two main system functions of MATLAB are used for iteration: ODE45.M and LSIM.M. The relative error level is controlled to be within 10^{-3}. In addition, some auxiliary computation tools are developed, which are used in the simulation for solutions to the final results. DV.M and SPL.M mainly enhance the functions of DIFF.M and SPLINE.M, respectively. RMS.M is developed using Simpson's rule to find various performance indices.

Both the main source file (only *frequency response* is given for reference) and utility functions are provided following the flow chart.

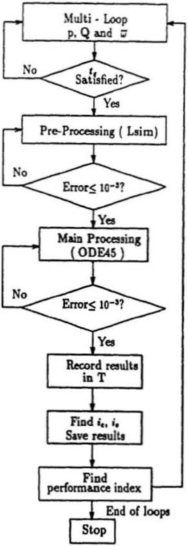

Figure A.1: Flow chart of simulation run based on Runge-Kutta algorithm.

Source programs for simulation run based on Runge-Kutta algorithm

The main program: SIMU.M

```
%%%%%%%%%%%%%%%%%%%%%%%%%%%%%%%%%%%%%%%%%%%%%%%%%%%%%%%%%%%%%%%
%                                                             %
%   Simulation Program for Performance Curves:  w | p,Q      %
%                                                             %
%%%%%%%%%%%%%%%%%%%%%%%%%%%%%%%%%%%%%%%%%%%%%%%%%%%%%%%%%%%%%%%

% I. Global Preparation
% ----------------------

clear
global   AA BB CC Q mm w xtam
format long

% II. Three Loops with w as variable and Q, p as parameters
% -----------------------------------------------------------

fail=1;
for p=0.6:0.1:1,          %%    δ = p * π

    if p==1,
       P=1;
     else
       P=10*p;
    end

    for Q=2:4:18,                  %% Quality factor of tank

     zz=[];

     for mn=1:10,    %% Frequency W = Ws / Wo

          if mn==1, w=1.06; end
          if mn==2, w=1.08; end
          if mn==3, w=1.1; end
          if mn==4, w=1.15; end
          if mn==5, w=1.2; end
          if mn==6, w=1.25; end
          if mn==7, w=1.3; end
          if mn==8, w=1.35; end
          if mn==9, w=1.5; end
          if mn==10, w=1.8; end

       ww=100*w;
```

```
% **** Check the turn-off angle condition ****
φ =atan(Q*(w-1/w));
% **** If the condition is not OK, turn to another w:
if abs( φ ) > (pi-p*pi)./2,
    fail=0;
%  Speed up to find the steady state result as initials
          t1=(0:pi/49:p*pi)';     t2=(0:pi/49:(1-p)*pi)';
          u1=ones(length(t1),1);   u2=ones(length(t2),1);

          AA=1e3; BB=10; CC=1e3;   x0=[0.182  -0.266 -3.284];
             xtam=pi/30;
          cs=0;        ct=0;        ctt=0;         x00=[1 1 1];

          a0=[ 0                       0                       0
               0           -(1/(Q*w))                 1/(Q*w)
               0           -(1/(w/Q))                      0 ];

          b=[1/(Q*w*CC)  0  0]';   c1=[1 0 0];   d=0;

          while cs < 20,

              if x0(3) <=0,   mm=1;
               else           mm=-1;
              end

              a=[-(1/(AA*BB))                  0       -(mm/(Q*w*CC))
                              0        -(1/(Q*w))             1/(Q*w)
              mm/(w/Q)        -(1/(w/Q))                           0];

            [y1,x1]=lsim(a,b,c1,d,u1,t1,x0);
            x0=x1(length(x1),:);

        if p~=1,
              [y2,x2]=lsim(a0,b,c1,d,u2,t2,x0);
               x0=x2(length(x2),:);
        end

              for i=1:3,
                  if abs(x0(i)) > abs(x00(i)),
                  r(i)=abs(x00(i)) ./ abs(x0(i));
                else
                  r(i)=abs(x0(i))  ./ abs(x00(i));
                 end
              end
```

```
                error1=abs(1-min(r));
                if error1 > 1e-3,     cs=0;
                 else                 cs=cs+1;
                end

                x00=x0;

            end    %  **** End of while loop - 1 ****

%%%%%%%%%%%%%%%%%%%%%%%%%%%%%%%%%%%%%%%%%%%%%%%%%%%%%%%%%%%%%%%%%%%%%%
%%
%%   FINALIZATION OF XX  --- Formulation of the required
%%       --- Using Runge-Kutta method

ti=0;  ct=0;  ctt=0;  x=[];  xx=[];  x00=[ 1  1  1 ];

while ctt < 10,

    if x0(3) <=0,  mm=1;
             else           mm=-1;
    end

            if p~=1,
               [t1 x1] = ode45('rf',ti,ti+p*pi,x0);
               [cx1,rx1]=size(x1);
               x01=x1(cx1,:);
               mm=0;
               [t2 x2] = ode45('rf',ti+p*pi,ti+pi,x01);
               [cx2,rx2]=size(x2);
               ti=ti+pi; x0=x2(cx2,:);
               t=[t1(1:cx1-1); t2]; x=[x1(1:cx1-1,:); x2];
             else                                 %% pwm=0
               [t x] = ode45('rf',ti,ti+pi,x0);
               [cx,rx]=size(x);
               ti=ti+pi; x0=x(cx,:);
            end

             for i=1:3,
         if abs(x0(i)) > abs(x00(i)),
            r(i)=abs(x00(i)) ./ abs(x0(i));
          else
            r(i)=abs(x0(i))  ./ abs(x00(i));
         end
    end
```

```
        error=abs(1-min(r));

    if error > 1e-3,
                ct=0; xx=[];
              else
                ct=ct+1;
                if ct > 20,
                   ctt=ctt+1;
                   xx=[xx; spl([t x])];
                end
             end

             x00=x0;

     end                % **** End of while Loop - 2 ****

%
%       Solving for ic, io
%

il=xx(:,3);    uc=xx(:,4);
ic=(w/Q)*dv(uc);
io=il+ic;
xx=[xx ic io];

eval(['save Q',num2str(Q),'w',num2str(ww),'.',num2str(P),'
       xxx ascii']);

%%%%%%%%%%%%%%%%%%%%%%%%%%%%%%%%%%%%%%%%%%%%%%%%%%%%%%%%%%%%%%%%%%%%%%%
%
%  Solution to Idave, Ilrms/Ilmax, Po, Vcrms/Vcmax, Iorms, PF
%

% ***  Idave  ***

     Np=(2*pi/xtam)+1;   idp=xx(1:Np,2);
     Idave = mean(idp);

% ***  Ilrms/Ilmax  ***

     ilp=il(1:Np);
     Ilrms=rms(ilp);
     Ilmax=max(abs(ilp));

% ***  Vcrms/Vcmax  ***

     ucp=uc(1:Np);
     Vcrms=rms(ucp);
     Vcmax=max(abs(ucp));
```

```
% ***  Iorms  ***

    iop=io(1:Np);
    Iorms=rms(iop);

% ***  Po  ***

    Po=Ilrms .^2;

% ***  PF  ***

    PF=Po ./ (Vcrms*Iorms);

% ***  tq  ***        Eqns: tq > toff; Phil=wstq+(pi-delta)/2;

    tqq=(Phil-((pi-p*pi)./2)) ./pi ;     %  ( p.u.)

% ***  Output  ***

    yy=[w Idave Ilrms Ilmax Vcrms Vcmax Po PF tqq];
    zz=[zz; yy];           % zz set to zero outside this Q loop.

    end  %%%% End of the condition loop

    end                    % End of w Loop

    if fail==0,
          eval(['save P',num2str(P),'Q',num2str(Q),'.dat
                zz /ascii']);
    end

    fail=1;

  end                      % End of Q Loop
end                        % End of p Loop
```

Function of the state-space equation: RF.M

```
%%%%%%%%%%%%%%%%%%%%%%%%%%%%%%%%%%%%%%%%%%%%%%%%%%%%%%%%%%%%
%                                                          %
%   FUNCTION FILE REPRESENTING THE SYSTEM EQUATION         %
%              CALLED BY FREQSIMU.M                        %
%                                                          %
%%%%%%%%%%%%%%%%%%%%%%%%%%%%%%%%%%%%%%%%%%%%%%%%%%%%%%%%%%%%

function  sst = rf(xta,x)

QW=Q*w;

sst(1)= -(1/(AA*BB)) * x(1) + (1/(CC*QW)) * (- mm * x(3) +1 );

sst(2)=  (1/QW) * ( - x(2) + x(3));

sst(3)=  (Q/w) * ( mm * x(1) -  x(2));

%%%% END  %%%%
```

Utility function: **SPL.M**

```
%%%%%%%%%%%%%%%%%%%%%%%%%%%%%%%%%%%%%%%%%%%%%%%%%%%%%%%%%%%%%%%%%%%

     function sp=spl(x)

%
%  This function performs splining on X, given ti,
%  and returns the more finely spaced X (without
%  the last colume ( N.B. The 1st row of X is t )
%


   xta=x(:,1);

   xtai=xta(1):xtam:xta(length(xta));

   sp=xtai; lxtai=length(xtai);

   [c, r]=size(x);

   for k=2:r,

       sp=[sp; (spline(xta,x(:,k),xtai))];

   end

   sp=sp';

   clear xtai a b

%%%% END %%%%
```

Utility function: DIV.M

```
%%%%%%%%%%%%%%%%%%%%%%%%%%%%%%%%%%%%%%%%%%%%%%%%%%%%%%%%%%%%%%%%%%%%%%%%%%%%%%%%%%%%%%%%%%%%%%%%%%%%%%%%%%%%%%%%%%%%%%%%%%%%%%%%%%%%

function div=dv(Uc)

%
%  FUNCTION FILE TO DIFFERENTIATE A MATRIX
%

H=xtam;

sz=size(Uc);

N=sz(1);

NMI=N-1;

for i=2:NMI;

    DF(i)=(Uc(i+1)-Uc(i-1)) ./ (2*H);

end

DF(1)=(2*Uc(2)-1.5*Uc(1)-0.5*Uc(3)) ./ H;

DF(N)=(1.5*Uc(N)-2*Uc(N-1)+0.5*Uc(N-2)) ./ H;

div=DF';

%%%% END %%%%
```

Utility function: RMS.M

```
%%%%%%%%%%%%%%%%%%%%%%%%%%%%%%%%%%%%%%%%%%%%%%%%%
%                                               %
%  INTERGRATION OF FUNCTION BY Simpson's Rule   %
%                                               %
%%%%%%%%%%%%%%%%%%%%%%%%%%%%%%%%%%%%%%%%%%%%%%%%%

function Irms = rms(x)     % Irms = ?

% ----------------------------------------------

H = xtam; N = ( 2*pi/H ) + 1;   % H: Intl Step; N: # of Points

a = 17/48;  b = 59/48;  c = 43/48;  d = 49/48;  % Intl coeffs.

[r c] = size(x);

if r ~= 1,    x=x';   end

R = x(1:N) .^2;     K = H ./ ( 2*pi );

I1=[a*R(1) b*R(2) c*R(3) d*R(4) R(5:N-4) d*R(N-3) c*R(N-2)

b*R(N-1) a*R(N)];

Irms = sqrt( K .* sum(I1) );

%%%% END %%%%
```

A.2 Simulation program 2 using MAPLE and NAG based on characteristic roots method

This program is written in FORTRAN language using two commercial packages of NAG FORTRAN, and MAPLE, a formula solver. The flow chart of the simulation run is shown in Figure A.2. In the program, subroutine ROOT is used to find roots of the characteristic equation (r, s, ω), while SYSGEN and SYSMO do the iteration during the intervals I/III and II/IV, as described in Chapter 3, respectively.

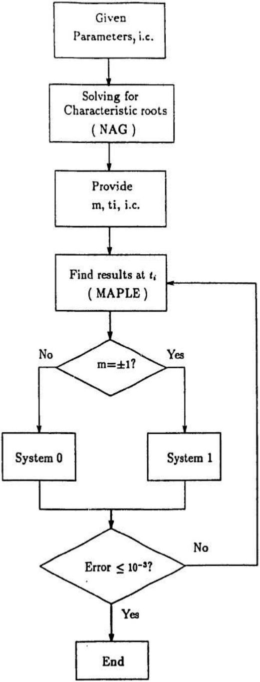

Figure A.2: Flow chart of simulation run with characteristic roots method.

Source program for simulation run based on characteristic roots method

```
cccccccccccccccccccccccccccccccccccccccccccccccccccccccccccccccccccc
c
c     SIMULATION PROGRAM  TO FIND SOLUTION TO SYSTEM EQUATIONS
c
c           --- Using Characteristic Roots Method
c
cccccccccccccccccccccccccccccccccccccccccccccccccccccccccccccccccccc

      IMPLICIT NONE
      REAL X,Y,Z,A,B,C,T,DIFF,X1,Y1,Z1,EPS,U,V,W
      REAL INC,PI,A1,Q,OM,M,R,S,W1,P,T1,T2
      INTEGER I,CONV,N,NC

         COMMON A1,Q,OM,R,S,W1
      OPEN (7,FILE='cycle.dat')

      CONV = 0

      nc=1e3
      a1=1e3
      eps=1e-3
      om=1.15
      p=0.8
      a=0
      b=0
      c=0

      WRITE(*,*)'ENTER NUMBER OF ALLOWED ITERATIONS'
      READ(*,*)NC
      WRITE(*,*)'ENTER A,Q,OMEGA,P,EPS'
      READ(*,*)A1,Q,OM,P,EPS
          M = 1.0
c     WRITE(*,*)'ENTER THE INITIAL VALUES'
c     READ(*,*)A,B,C
      CALL  ROOT(A1,Q,OM,M,R,S,W1)

      PI = 4.0*ATAN(1.0)
      T1 = PI*P
      T2 = PI - T1
      N = 100

c    M = + 1
      CALL SYSGEN(1.,X,Y,Z,A,B,C,T1)

      DO 10 I = 1,NC
```

```
C   M = 0
         A = X
         B = Y
         C = Z
         CALL SYSMO(X1,Y1,Z1,A,B,C,T2)

C   M = -1
         A = X1
         B = Y1
         C = Z1
         CALL SYSGEN(-1.,U,V,W,A,B,C,T1)

C   M = 0
         A = U
         B = V
         C = W
         CALL SYSMO(U,V,W,A,B,C,T2)

C   M = +1
         A = U
         B = V
         C = W
         CALL SYSGEN(1.,X1,Y1,Z1,A,B,C,T1)

         DIFF = SQRT((X-X1)**2+(Y-Y1)**2+(Z-Z1)**2)

         IF (DIFF.LT.EPS) THEN
              CONV=1
              GOTO 100
         ELSE
              X=X1
              Y=Y1
              Z=Z1
         write(*,*)diff,i,x,y,z
         ENDIF

10   CONTINUE
100  IF (CONV.EQ.1) THEN
         WRITE(*,*)'CONVERGED AT ',I,' ITERATIONS'

         WRITE(7,*) X,Y,Z

              INC = T2/N
         T = 0.
```

```
          DO 11 I=1,N+1
               CALL SYSMO(U,V,W,X,Y,Z,T)
               WRITE(7,*)U,V,W
               T = T + INC

11        CONTINUE
          T= 0.
               INC = T1/N
          DO 12 I=1,N+1
               CALL SYSGEN(-1.,X,Y,Z,U,V,W,T)
               WRITE(7,*)X,Y,Z

               T = T + INC

12        CONTINUE

          T = 0.
               INC = T2/N
          DO 13 I=1,N+1
               CALL SYSMO(U,V,W,X,Y,Z,T)
               WRITE(7,*)U,V,W
               T = T + INC

13        CONTINUE

          T= 0.
               INC = T1/N

          DO 14 I=1,N+1
               CALL SYSGEN(1.,X,Y,Z,U,V,W,T)
               WRITE(7,*)X,Y,Z
               T = T + INC

14        CONTINUE

      ELSE
          WRITE(*,*)'DID NOT CONVERGE'
      ENDIF

      END
```

```
SUBROUTINE SYSGEN(M,X,Y,Z,X00,Y00,Z00,T)
IMPLICIT NONE
REAL A1,Q,OM,X0,Y0,Z0,M,X,Y,Z,T,AN,AD,CN
REAL T7,T6,T8,T9,T10

REAL A,B,C,D,F,G,H,I,R,S,W
REAL X00,Y00,Z00
COMMON A1,Q,OM,R,S,W


x0 = x00 -1./m**2
y0 = y00 - 1./m
z0 = z00 - 1./m

an=(om**2*r**2*q-om*r+q)*(-q*om**2*a1*s**2*x0-q*x0*om**2
     *w**2*a1#-y0*m*q+m**2*q*x0+2*om*s*z0*m)

ad =q*om*(m**2*om*r**2*q-m**2*r-om**3*s**2*a1*r**2*q+om**2
     *s**2**  #1*r-q*om*s**2*a1-om**3*w**2*a1*r**2*q+om
     **2*w**2*a1*r-q*om*w**2*a1#-2*om*s*m**2*q*r+2*m**2*s)

cn = -(-r**2*a1*s*y0*om**3*q**2-r**2*q*om**4*z0*w**2*a1+r
     **2*q*om*#*4*a1*s**2*z0+r**2*q*om**2*z0*m**2+r*q**2*om
     **3*a1*s**2*m*x0-r*q**#2*om**3*m*x0*w**2*a1+r*q**2
     *om*m**3*x0-r*q**2*om*m**2*y0+r*a1*s*y0#*om**2*q+r
     *om**3*z0*w**2*a1-r*om**3*a1*s**2*z0-r*z0*m**2*om-q**2*o
     #m*a1*s*y0+q**2*om*a1*s*m*x0-q*om**2*z0*w**2*a1-q*om
     **2*a1*s**2*m*x#0+q*om**2*a1*s**2*z0+q*om**2*m*x0*w**2
     *a1-q*m**3*x0+q*m**2*y0)*m/w#/om/a1

a = an/ad
b = x0 - a
c = cn/ad
d = 1/(om**2*r**2*q-om*r+q)*m*a*q
f = -q*om/m/(-1+q*om*s)
f = f*(w*m**2*b+om**2*w*s**2*a1*b-2*om**2*w**2*s*a1*c-om
     **2*w**3
     # *a1*b+b*a1*w+a1*c*s)
g = a1*q*om*a*r/m
h = z0 - g
i = (b*w+c*s)*a1*q*om/m
t6 = exp(-r*t)
t7 = exp(-s*t)
t8 = w*t
t9 = t7*cos(t8)
t10 = t7*sin(t8)
x = a*t6+b*t9+c*t10 + 1./m**2
y = d*t6+(y0-d)*t9+f*t10 + 1./m
z = g*t6+h*t9+i*t10+ 1./m

RETURN
END
```

```
      SUBROUTINE SYSMO(X,Y,Z,X0,Y0,Z0,T)
      IMPLICIT NONE
      REAL X,Y,Z,X0,Y0,Z0,T,T3,T4,T5,E,F,H,I
      REAL A1,Q,OM,S1,W1,R,T2,S,W
      COMMON A1,Q,OM,R,S1,W1

      s = 1/om/q/2
      t2 = q**2
      t5 = sqrt(-1+4*t2)
      w = s*t5
      e = y0
      f = 1/q/om/w*(z0-y0+q*om*y0*s)
      h = z0
      i = -q*om*e*w-q*om*f*s+f
      t3 = exp(-s*t)
      t4 = w*t
      x = t/(a1*q*om) + x0
      y = e*t3*cos(t4)+f*t3*sin(t4)
      z = h*t3*cos(t4)+i*t3*sin(t4)

      RETURN
      END

       SUBROUTINE ROOT(A1,Q,OM,M,R,S,W)
C     C02ADF EXAMPLE PROGRAM TEXT
C     MARK 13 REVISED. NAG COPYRIGHT 1988.
C     .. Parameters ..
      INTEGER          NMAX
      PARAMETER        (NMAX=20)
      INTEGER          NIN, NOUT
      PARAMETER        (NIN=5,NOUT=6)
C     .. Local Scalars ..
      DOUBLE PRECISION PI, TOL
      REAL A1,Q,OM,M
      INTEGER           I, IFAIL, N, NA, T
C     .. Local Arrays ..
      DOUBLE PRECISION AC(NMAX), AR(NMAX), IMZ(NMAX), REZ(NMAX)
C     .. External Functions ..
      DOUBLE PRECISION A02ABF, X01AAF, X02AJF
      EXTERNAL          A02ABF, X01AAF, X02AJF
C     .. External Subroutines ..
      EXTERNAL          C02ADF
C     .. Intrinsic Functions ..
      INTRINSIC         COS, SIN

C     .. Executable Statements ..

      PI = X01AAF(PI)
      TOL = X02AJF()
      N = 4
      AR(4) = M**2
      AR(3) = -(A1+M**2)*Q*OM
      AR(2) = A1*OM**2
      AR(1) = -A1*OM**3*Q
```

```
      DO 19 I = 1,N
      AC(I) = 0.0
19    CONTINUE
.
         WRITE (NOUT,FMT=99995) N - 1
         DO 20 I = 1, N
            WRITE (NOUT,FMT=99998) AR(I), AC(I)
20    CONTINUE
         T = 0
         NA = N
         IFAIL = 1
40    CALL C02ADF(AR,AC,NA,REZ,IMZ,TOL,IFAIL)
         IF (IFAIL.EQ.2) THEN
            IF (T.LT.N) THEN
               T = T + 1
               REZ(1) = (1.1D0**T)*0.15D0*COS(2*T*PI/N)
               IMZ(1) = (1.1D0**T)*0.15D0*SIN(2*T*PI/N)
               GO TO 40
            ELSE
               WRITE (NOUT,FMT=99996) T
            END IF
         ELSE IF (IFAIL.NE.0) THEN
            WRITE (NOUT,FMT=99997) IFAIL
            STOP
         END IF
         WRITE (NOUT,FMT=99994)
         DO 60 I = N - 1, NA, -1
            WRITE (NOUT,FMT=99998) REZ(I), IMZ(I), A02ABF(REZ(I),
     IMZ(I))
60    CONTINUE
       R = REZ(3)
       S = REZ(2)
       W = IMZ(2)
       WRITE(*,*)'r,s,w',R,S,W

C

99998 FORMAT (' ',3(D13.4,2X))
99997 FORMAT (/' C02ADF EXITS WITH IFAIL =',I3)
99996 FORMAT (/' C02ADF EXITS WITH IFAIL = 2 AFTER',I4,' RESTARTS')
99995 FORMAT ('POLYNOMIAL ORDER',I6,//'
COEFFICIENTS OF POLYNOMIAL',
     *  //'    REAL PART    IMAGINARY PART',/)
99994 FORMAT (/' ROOTS OF POLYNOMIAL',//'    REAL PART    IMAGINARY
PA',
     *  'RT     MODULUS',/)
      RETURN
      END
```

Appendix B

System Performance Evaluation in Two Other Formats

In this appendix two more sets of performance curves based on the simulation results are provided. They are essentially the same in nature as those included in Chapter 3, but in other formats to highlight the performance of the PWM CSI inverters with respect to other parameters.

Figure B.1 to B.6 describe the load characteristics of the inverter system, or the *Load Effect*. The PWM control index, p on the X-axis describes the *Control Effect* in Figure B.7 to B.10. They can also be used for design purpose.

B.1 Load effect evaluation (Figure B.1 - B.6)

B.2 Control effect eveluation (Figure B.7 - B.10)

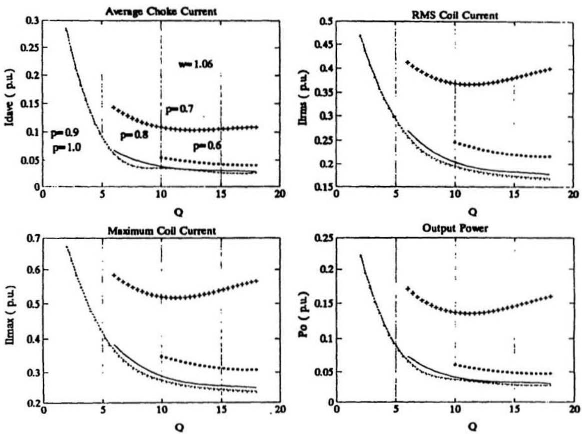

Figure B.1: Simulation results: Load Effect of $\overline{I_{dave}}$, $\overline{I_{Lrms}}$, $\overline{I_{Lmax}}$ and $\overline{P}_o$ with $\overline{\omega} = 1.06$.

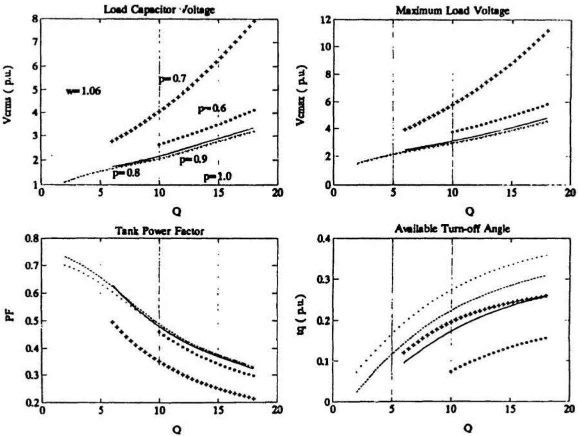

Figure B.2: Simulation results: Load Effect of $\overline{V_{crms}}$, $\overline{V_{cmax}}$, PF, and $\overline{t_{qq}}$ with $\omega_o = 1.06$

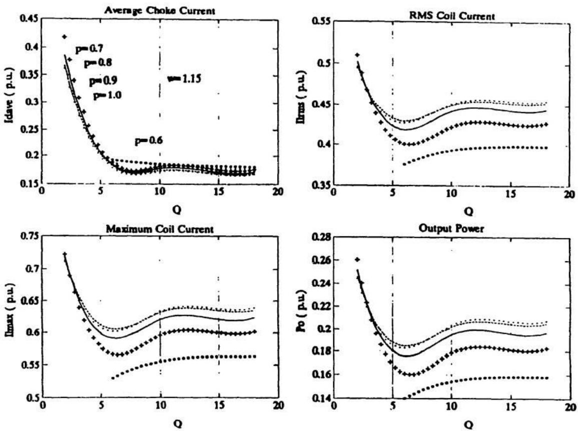

Figure B.3: Simulation results: Load Effect of $\overline{I_{dave}}$, $\overline{I_{Lrms}}$, $\overline{I_{Lmax}}$ and $\overline{P_o}$ with $\overline{\omega} = 1.15$.

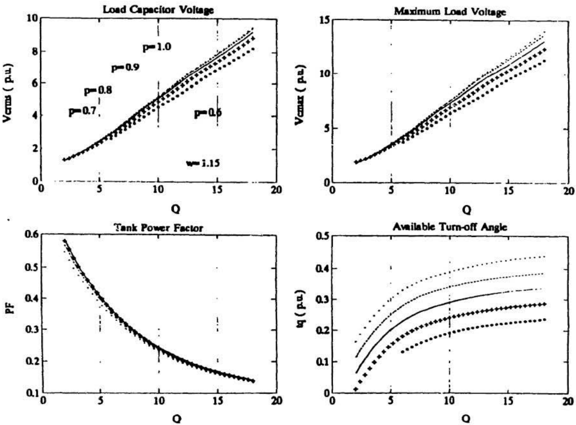

Figure B.4: Simulation results: Load Effect of $\overline{V_{crms}}$, $\overline{V_{cmax}}$, PF, and $\overline{t_{qq}}$ with $\omega_o = 1.15$

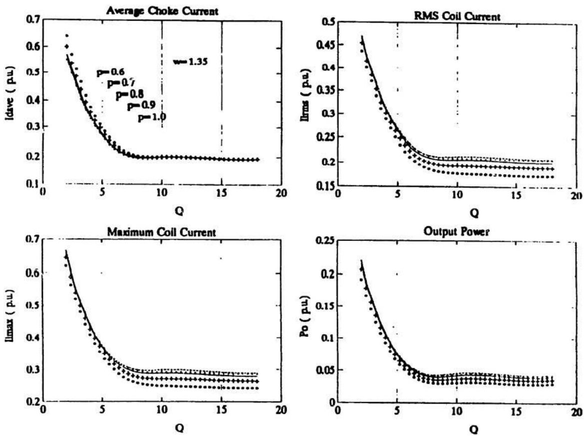

Figure B.5: Simulation results: Load Effect of $\overline{I_{dave}}$, $\overline{I_{Lrms}}$, $\overline{I_{Lmax}}$ and $\overline{P_o}$ with $\overline{\omega} = 1.35$.

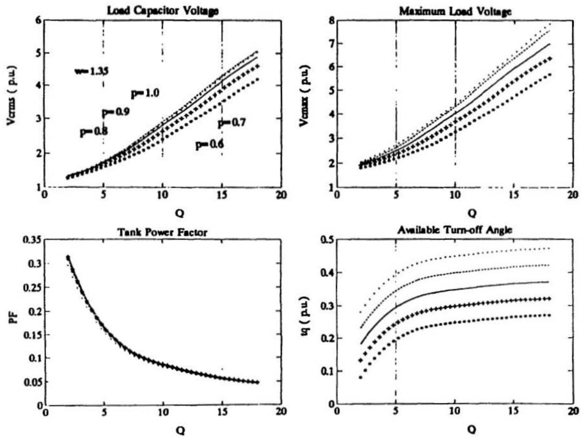

Figure B.6: Simulation results: Load Effect of $\overline{V_{crms}}$, $\overline{V_{cmax}}$, PF, and $\overline{t_{tq}}$ with $\omega_o = 1.35$

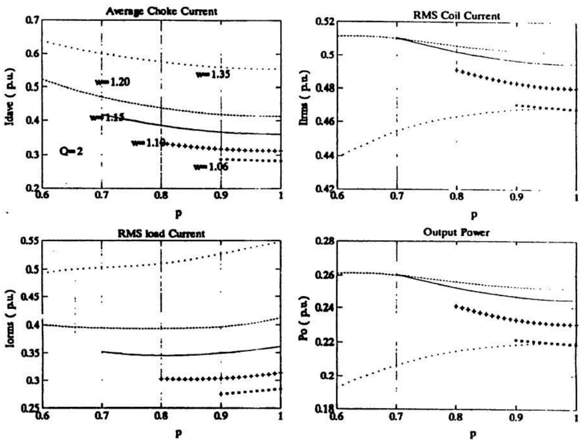

Figure B.7: Simulation results: Load Effect of $\overline{I_{dave}}$, $\overline{I_{Lrms}}$, $\overline{I_{Lmax}}$ and $\overline{P_o}$ with $Q = 2$.

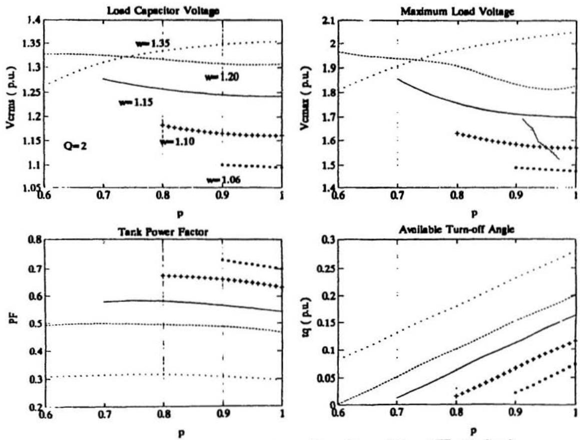

Figure B.8: Simulation results: Load Effect of $\overline{V_{crms}}$, $\overline{V_{cmax}}$, PF, and $\overline{t_{qq}}$ with $Q = 2$.

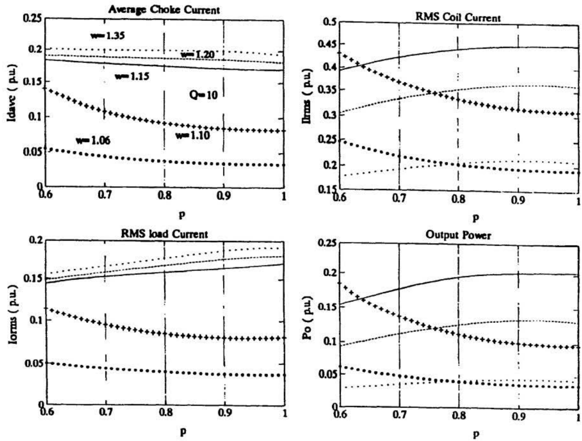

Figure B.9: Simulation results: Load Effect of $\overline{I_{dave}}$, $\overline{I_{Lrms}}$, $\overline{I_{Lmax}}$ and $\overline{P_o}$ with $Q = 10$.

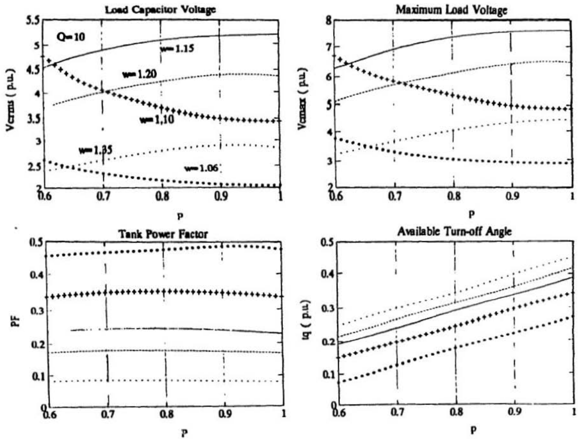

Figure B.10: Simulation results: Load Effect of $\overline{V_{crms}}$, $\overline{V_{cmax}}$, PF, and $\overline{t_{tq}}$ with $Q = 10$.

Appendix C

Configuration of the PWM Triggering Circuit

In order to describe the triggering circuit in more detail, Figure 4.2 of Chapter 4 is included again here in Figure C.1 for reference.

The production of the required signals is obtained by comparison of a sawtooth waveform with two reference DC voltage levels. Phase shift is made available when one of the DC level is moving above the other, or the base reference voltage V_B. An IC chip of XR-2207, which is a versatile VCO with quite satisfactory functions, is chosen to serve as the main pulse source of the sawtooth waveforms. Resistors of 28K and 3.3K are connected to pin 5 and 6, respectively, in order to result in the nearly sawtooth waveform in pin 14, as shown in Figure C.2.

Two LM311 IC's function as voltage comparators which give dual rectangular waveforms with a phase difference based upon the two reference voltages, V_B and V_M. The falling edges of the two waveforms are aligned and thus the other sides form the phase difference.

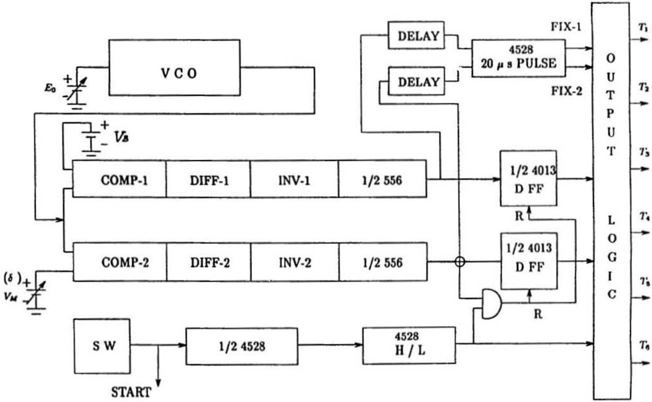

Figure C.1: Block diagram of the triggering circuit.

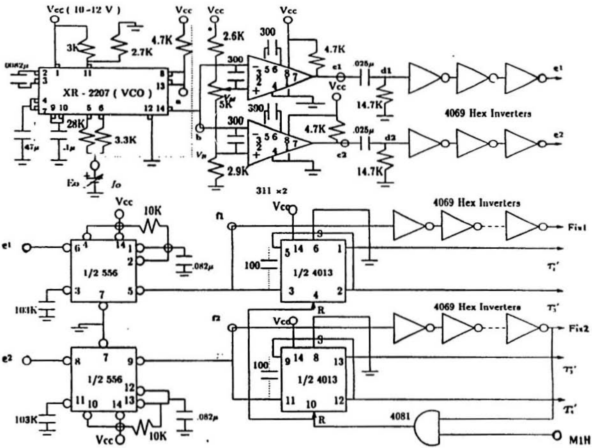

Figure C.2: Triggering circuit diagram: Part-1.

The outputs of 311's go through two separate channels composed of an RC differentiator followed by three inverters in series. The results are used to trigger two 556's function generators, which produce pulses of about $100\mu s$ in width. These pulses then reliably initialize a 4013 chip (dual D flip-flop's). The D flip-flop is used here because of its ability of giving simultaneously two pulses of opposite polarities, which happen to satisfy the need of the final triggering of two pairs of thyristors.

As stated before, the signals supposed to trigger the thyristors should come into a pulse transformer first. The ideal width of the pulses is about $20\mu s$. Therefore outputs from the D flip-flop's cannot be used directly with the transformer. This is solved by letting the rectangular waveforms from 4013 be ANDed with two series of $20\,\mu s$ pulses at the output logic network. Those pulses are obtained from the output of 566's followed by series-connected six inverters that produce some delays so that the waveforms could reliably be ANDed, and then they trigger two other 4528's to get the final $20\mu s$ pulses. This is illustrated in Figure C.3, where the mode control circuit and output logic circuit are also presented.

In Figure C.3, 4528 square-wave generators are used to form the mode control signals. The principle of starting process is illustrated in Figure 4.1 in Chapter 4. The function of Mode-1 and Mode-2 circuits is to have T_5 and T_6 invoked temporarily until enough electrical quantities are built up in the tank so that commutation is possible. Mode-3 indicates the steady-state operation of the inverter. The first half of 4528 is connected to a switch to help form the START signal. Another 4528 chip makes two circuits that give both Mode-1 High/Low and Mode-2 H/L signals. The durations of the two pulses are

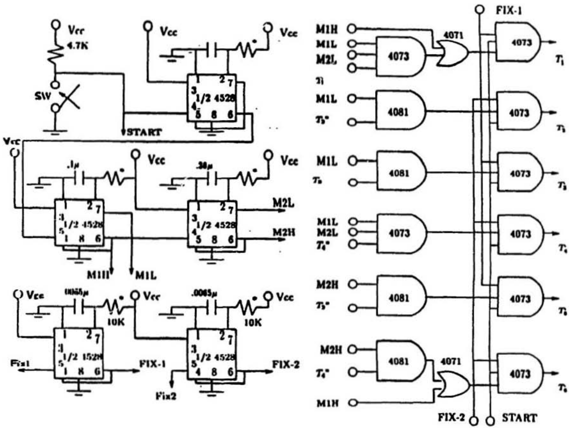

Figure C.3: Triggering circuit diagram: Part-2.

determined by the product of resistance and capacitance in the circuits. The last 4528 chip is used to produce the final FIX-1 and FIX-2 signals for the AND operation. The resultant output logic circuit is given in Figure C.3. All the theoretical waveforms showing the steady-state working principle of this triggering circuit are illustrated in Figure C.4. The waveforms are not the results of simulation and no scales are considered, since the synthesis of all the waves is relatively staightforward.

Finally, experimental waveforms for verification are provided in Figure C.5 and C.6.

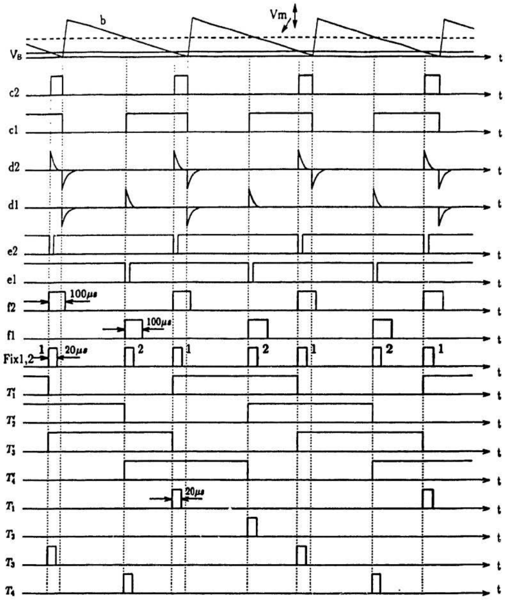

Figure C.4: Relevant waveforms of triggering circuit in steady-state.

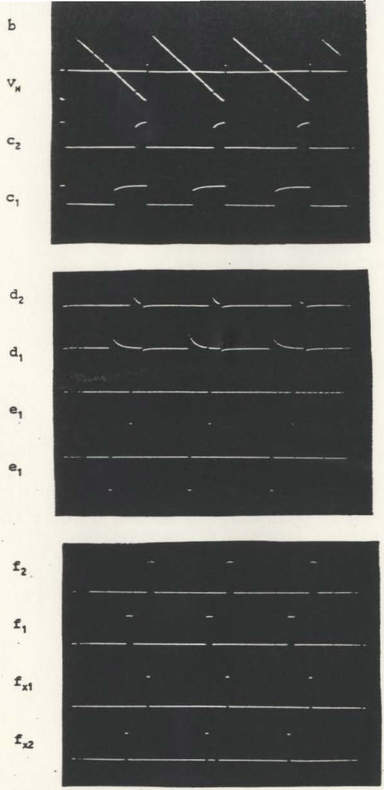

Figure C.5: Experimental waveforms for verifications: Waveforms of points b, V_M, c_2, c_1, d_2, d_1, e_2, e_1, f_2, f_1, f_{x_1} and f_{x_2}. X-axis: $0.24ms/div.$; Y-axis: $10Volts/div$.

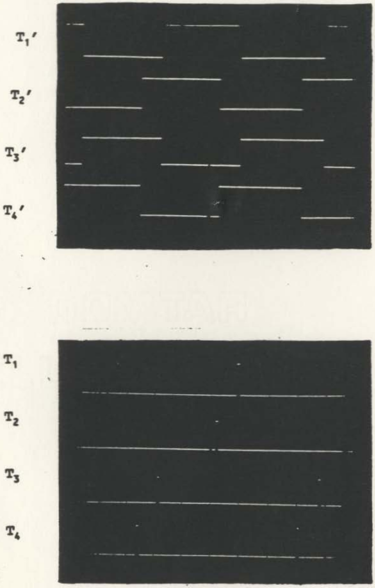

Figure C.6: Experimental waveforms for verifications: Waveforms of points T_1', T_2', T_3', T_4', T_1, T_2, T_3, and T_4. X-axis: $0.24ms/div.$; Y-axis: $10Volts/div.$